공학박사학위논문

Superhydrophobicity of Textile Membrane with Hierarchical Structured Roughness

계층적 구조의 거칠기를 가진 텍스타일 멤브레인의 초소수성 구현

2017년 2월

서울대학교 대학원

재료공학부

정 선 아

Superhydrophobicity of Textile Membrane with Hierarchical Structured Roughness

계층적 구조의 거칠기를 가진 텍스타일 멤브레인의 초소수성 구현

지도교수 **강 태 진**

이 논문을 공학박사 학위논문으로 제출함

2016 년 12 월

서울대학교 대학원

재료공학부

정 선 아

정 선 아의 공학박사 학위논문을 인준함

2017 년 1 월

위 원 장 _____ (인)

부위원장 _____ (인)

위 원 _____ (인)

위 원 _____ (인)

위 원 _____ (인)

ABSTRACT

Superhydrophobicity of Textile Membrane with Hierarchical Structured Roughness

Seon Ah Jeong
Department of Materials Science and Engineering
The Graduate School
Seoul National University

Superhydrophobic surfaces have drawn a lot of interest both in academia and in industry because of the usability and their wide applications. Inspired by the extreme wetting states displayed by the natural materials, superhydrophobic surfaces have been widely fabricated by various techniques. In this work, superhydrophobic surfaces were manufactured by the spray-coating the hydrophobized silica nanoparticles on cotton textiles and superhydrophobic polyvinylidene fluoride webs were produced by electrospinning.

First of all, superhydrophobic and transparent surfaces on the cotton fabrics have been developed using the silica nanomaterials. Initially, trichlorododecylsilane was treated on the silica nanoparticles to lower the surface energy of the fabric. By simply spraying alcohol suspensions containing hydrophobized silica nanoparticles, the extremely water repellent coatings were formed on the textile fabrics. The effect of three type of alcohol solvent on the hydrophobicity of the coated cotton fabrics were examined by measuring the surface wettability. The treated cotton textiles in methanol exhibited the extremely water-repellent behavior with the water contact angles higher than 170° and the contact angle hysteresis lower than 10°. It proved

to be essential to form the hierarchical morphology in achieving superhydrophobicity.

Then, highly hydrophobic electrospun poly(vinylidene fluoride) (PVDF) films have been developed from the electrospinning system by controlling the surface morphology. The PVDF was dissolved in a solvent with different concentrations of 8, 12, 16, and 20 w/v% to investigate the effect of the viscosity on the surface roughness and the hydrophobicity of the electrospun webs. The PVDF material was used due to its low surface energy, thus showing the inherent hydrophobicity. By controlling the surface structure by changing the concentrations, the PVDF webs with the hierarchical morphology, both nanometer- and micrometer-sized roughness, were successfully obtained. The beaded fiber structures with nano-sized fibers and micro-scaled beads and the highest roughness factor about 1.2μm were formed and that surface exhibited the contact angles about 150° with the contact angle hysteresis of 11°, and showing good water repellency. The fabricated PVDF membranes also showed the good oil-water separation ability and oil absorption capabilities as well, demonstrating as the stable oil sorbent material. With the excellent mechanical properties, the electrospun superhydrophobic PVDF membrane is expected to be applied to industrial oil-polluted water treatment material.

Keywords: Superhydrophobicity, Inorganic coating, Electrospinning, Hierarchical roughness, Smart composites

Student Number: 2012-24166

CONTENTS

List of Figures

Figure 11. Schematic view of the captive method for hysteresis measurement. Advancing contact angles measurement (a) and receding contact angles measurement (b).

Figure 12 X-ray photoelectron spectroscopy results of (a) the fumed silica and (b) modified silica nanoparticles with dodecyltrichlorosilane.

Figure 13. NMR spectra of (a) the fumed silica and (b) modified silica nanoparticles with dodecyltrichlorosilane.

Figure 14. Captured images of the water droplets (3 μL) placed on the cotton fabrics showing the CAs and the specifications. (a) Pristine cotton fabric, (b) cotton fabric coated in 1-propanol (c) cotton fabric coated in ethanol (d) cotton fabric coated in methanol.

Figure 15. Water contact angles of pristine and the cotton fabrics coated with silica nanoparticles in 1-propanol, ethanol, and methanol.

Figure 16. Photographs of captive method for hysteresis (a) at start point, (b) advancing point, and (c) receding point of the cotton fabrics coated with silica nanoparticles in 1-propanol. Graph the advancing and receding angle values (d).

Figure 17. Photographs of captive method for hysteresis (a) at start point, (b) advancing point, and (c) receding point of the cotton fabrics coated with silica nanoparticles in ethanol. Graph the advancing and receding angle values (d).

Figure 18. Photographs of captive method for hysteresis (a) at start point, (b) advancing point, and (c) receding point of the cotton fabrics coated with silica nanoparticles in methanol. Graph the advancing and receding angle values (d).

Figure 19. Advancing and receding contact angles of the cotton fabrics coated with silica nanoparticles in 1-propanol, ethanol, and methanol, respectively measured by the captive method.

Figure 20. SEM images of SiO_2 NPs-covered cotton fabrics. The images on the left are low-magnification ones and that on the light are high-magnification ones. (a) pristine cotton fibers, (b) the cotton fibers coated in 1-propanol, (c) the cotton fibers coated in ethanol, (d) the cotton fibers coated in methanol.

Figure 21. Particle size distribution of suspension containing the silica nanoparticles using methanol (red line), ethanol (blue line), and 1-propanol (green line). The average particle sizes are 629, 486, and 412 nm, respectively.

Figure 22. Dispersion ability of superhydrophobic treated silica nanoparticles in methanol, ethanol, and 1-propanol detected using UV-vis spectrophotometer at 600 nm.

Figure 23. Water contact angles (a) and sliding angles (b) of the superhydrophobic treated cotton fabric after washing treatment with and without detergent.

Photographs of dynamic measurements of water adhesion of (a) the cotton fabrics coated with silica nanoparticles in methanol and (b) the pristine cotton textile.

Figure 24. Biphasic Janus cotton fabric. (a and c) water droplet images and contact angles of the back side from spray-coated cotton textile (a) and (c) up side, respectively. (b) Photograph of the free-standing biphasic Janus fabric displaying antisymmetric wetting behavior.

Figure 25. Photographs of dynamic measurements of water adhesion of (a) the cotton fabrics coated with silica nanoparticles in methanol and (b) the pristine cotton textile.

Figure 26. Photographs of (a) pristine cotton fabric and (b) coated cotton fabric by silica nanoparticles in methanol on which a water droplet maintained a spherical form. Red square area indicated a region of water absorbed.

Figure 27. Photographs of water droplets with the three different volumes, 5, 10, 30 μl from the left to the right on a cotton fabric coated by silica nanoparticles using methanol. (a) side view; (b) top-down view.

Figure 28. Chemical structure of polyvinylidene fluoride (PVDF).

Figure 29. FE-SEM images of PVDF fibrous films by electrospinning of (a) 8 wt%, (b) 12 wt%, (c) 1 6wt%, and 20 wt% concentrations. SEM micrograph magnification is 3,000 x.

Figure 30. The fiber diameter distributions diagram and the average size of the

surface morphology of (a) 8 wt%, (b) 12 wt%, (c) 16 wt%, and (d) 20 wt% concentrations of electrospinning solutions.

Figure 31. Steady flow curves of (a) shear stress and (b) shear viscosity with respect to the varying shear rate for the PVDF solutions from the different PVDF concentrations.

Figure 32. AFM 3D images and cross-sectional profiles in a given location of electrospun PVDF membrane surface with different concentrations (a) 8 wt%, (b) 12 wt%, (c) 16 wt%, and (d) 20 wt%.

Figure 33. Captured images of the water droplets at varying volumes 1, 3, 5, 10μL placed on the electrospun PVDF fibrous web from the (a) 8wt%, (b) 12 wt%, (c) 16wt%, and (d) 20 wt% concentration solution.

Figure 34. Water contact angles of the electrospun PVDF fibrous films of varying concentrations from 8wt% to 20wt% at the different water droplet volumes from 1μL to 10μL.

Figure 35. Effect of the surface roughness and concentrations of PVDF on the static water contact angle.

Figure 36. Advancing and receding angles respect to tilting angle of the electrospun PVDF films from (a) 8wt%, (b) 12wt%, (c) 16wt%, and (d) 20wt% solutions.

Figure 37. FE-SEM image of the PVDF flat film with 16wt% concentrations by solvent casting method (a) and the electrospinning process (b). The captured images of the water droplets of 3μL placed on the solvent casted film (c) and the electrospun web (d).

Figure 38. EDS spectrum of (a) the electrospun PVDF web, (b) the solvent casted PVDF film, and (c) surface chemical composition of each.

Figure 39. FT-IR spectra of the solvent-casted PVDF film and electrospun PVDF web

Figure 40. α and β phase content in the solvent-casted PVDF film and electrospun PVDF web (a) and ratio of the β-phase to α-phase of PVDF membranes.

List of Tables

Ⅰ. Introduction

1.1 General Background

The wetting behavior of a solid surface against any liquid is a crucial for surface property which plays important roles in industry and daily life. Typically, the surfaces are considered to be superhydrophobic if they exhibit extraordinarily high-contact angles higher than 150° and low contact-angle hysteresis between advancing and receding contact angles, typically less than 10°. These surfaces with special wettability have aroused much interest due to their non-adhesive and non-wetting features and various applications of multifunctional materials, such as self-cleaning, anti-corrosion, anti-icing, low hydrodynamic friction, and templates for directed self-assembly of nanomaterials, microfluidic and nanofluidic materials and devices [1, 2].

It is well known that many surfaces exist with highly hydrophobic and self-cleaning property in nature. For example, the wings of butterfly and the leaves of plants have the excellent water-repellent properties because of their surface structure and chemistry, and consequently, water droplets are instantly repelled from or roll off them. The best known example of a superhydrophobic and self-cleaning surface is the lotus leaf in **Figure 1(a)**. The lotus leaves possess strong water repellent properties that enhance the mobility of rain drops, carrying dirt away, and creating a self-cleaning effect, so-called “lotus effect”. The lotus effect, as shown in **Figure**

1b, describes the excellent super-antiwetting and self-cleaning ability of lotus leaf surfaces. The rainwater can smoothly roll off the lotus leaves instead of sticking to the surface and collect all dirt and parasites on their way. These special characteristics are attributed to the combination of a waxy layer with low surface energy and dual-scale rough structured surface with protrusions on lotus leaves.

Neinhaus and Barthlott first discovered the superhydrophobicity and patented it in 1998 as the lotus effect [3]. They obtained the scanning electron microscope (SEM) images for several water-repellent plants and reported the micro morphological characteristics of 200 species. The authors demonstrated that the epidermal, outermost, cells of the lotus leaves form papillae, which act as microstructure roughness, as shown in **Figure 1(c)**.

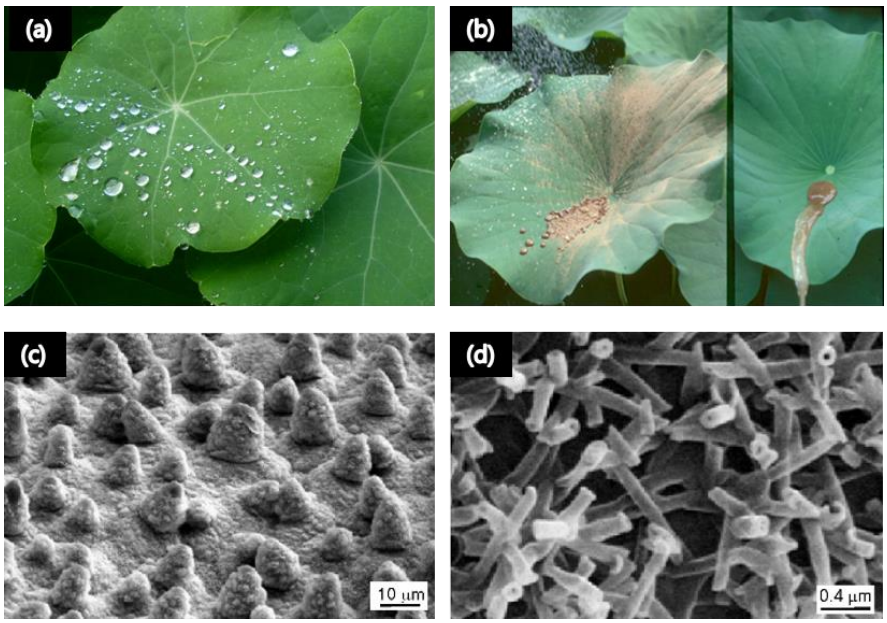

Figure 1. (a) A lotus leaf, known for its exceptional water repellency and (b) with self-cleaning effect. (c, d) Two different magnification of scanning electron microscope images showing hierarchical morphology of micro- and nanostructures [4].

The papillae are superimposed by a very dense layer of epicuticular waxes (wax crystals), also referred to as nanostructure roughness (**Figure 1(d))** [4]. Due to this double-scale roughness and the low surface tension of crystals, water easily rolls off and picks up dust. Thus lotus leaves are always clean. This combination results in static contact angles on lotus leaves exceeding 150 degrees and excellent low sliding angle. Because of the micro- and nanostructure roughness, the contact area between dirt particles and the leaf's surface is dramatically reduced. If the lotus leaf surface is tilted, even with a slight angle, water droplets begin to roll off the leaves, and thus collect and remove dirt from the surface, which is a self-cleaning effect.

To mimic these biological superhydrophobic features, many artificial surfaces have been engineered and manufactured worldwide. **Figure 2** indicates the methods available to achieve superhydrophobic surfaces by using two combined strategies, one related to changes in surface energy and the other one related to changes in surface roughness. In summary, superhydrophobic surfaces can be produced in two ways: by creating a rough surface on a hydrophobic surface and also by modifying the existing rough surface with materials of low surface energy, such as with fluorination or the addition of silicon compounds.

Materials with low surface energy include fluorocarbons, silicones, and some organic and inorganic materials. Fluorocarbons are of particular interest due to their extremely low surface energy. Roughening these polymers in certain ways leads to superhydrophobicity directly. Although fluorocarbons show the lowest surface energy known, it is interesting to note that they are rarely present in the organic materials produced by nature. Silicones are other widely used low surface energy

materials. They have also attracted industrial interest. Although fluorocarbons and silicones are known as hydrophobic materials, nature achieves non-wetting and self-cleaning using paraffinic hydrocarbons. Organic materials such as polyamide, polycarbonate, polyethylene and polystyrene have been made into suiperhydrophobic surface. Also, certain inorganic materials have been made into superhydrophobic surfaces. For example, superhydrophobic surfaces have been produced from ZnO, TiO_2, and SiO_2, etc.

The hierarchical roughness can be created through etching and lithography, sol-gel processing, layer-by-layer and colloidal assembly, electrochemical reaction and deposition, electrospinning and phase separation. Up to now, many articles have reported to produce rough surfaces including solidification of melted alkylketene dimer (AKD, a kind of wax) [5], plasma polymerization/etching of polypropylene (PP) in the presence of polytetrafluoroethylene (PTFE) [6], microwave plasma-enhanced chemical vapor deposition (MWPE-CVD) of trimethylmethoxysilane (TMMOS) [7], anodic oxidization of aluminum [8], immersion of porous alumina gel films in boiling water [9], mixing of a sublimation material with silica or boehmite [10], phase separation [11], molding [12], layer-by-layer deposition [13], sol–gel method [14], and electrospinning [15]. In this study, the superhydrophobic surfaces have been developed from more simple, rapid and inexpensive approaches for the mass application in industrial fields.

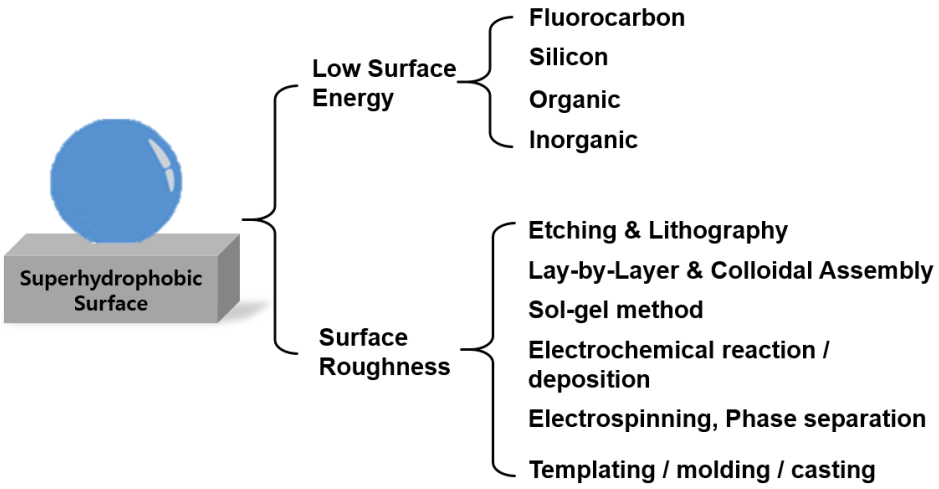

Figure 2. Strategies used to achieve superhydrophobicity by combining low surface energy materials and surface roughness.

1.2 Theory of Superhydrophobicity

Wettability of solid surfaces has been studied for a very long time. The wetting behavior of solid surfaces can be divided into four classes, defined by their static contact angle and as shown in **Figure 3**. Surfaces are termed as superhydrophilic when the contact angles are less than 10°. Surfaces with contact angles more than 10° and less than 90° are termed as hydrophilic. Hydrophobic surfaces have high contact angles, which means that the liquid on the surface forms a semi-spherical or spherical droplet, and the CA is more than 90° and less than 150°. If a surface has a static contact angle of more than 150° and a low hysteresis or a low tilting angle of less than 10°, they are called as superhydrophobic and can provide self-cleaning properties.

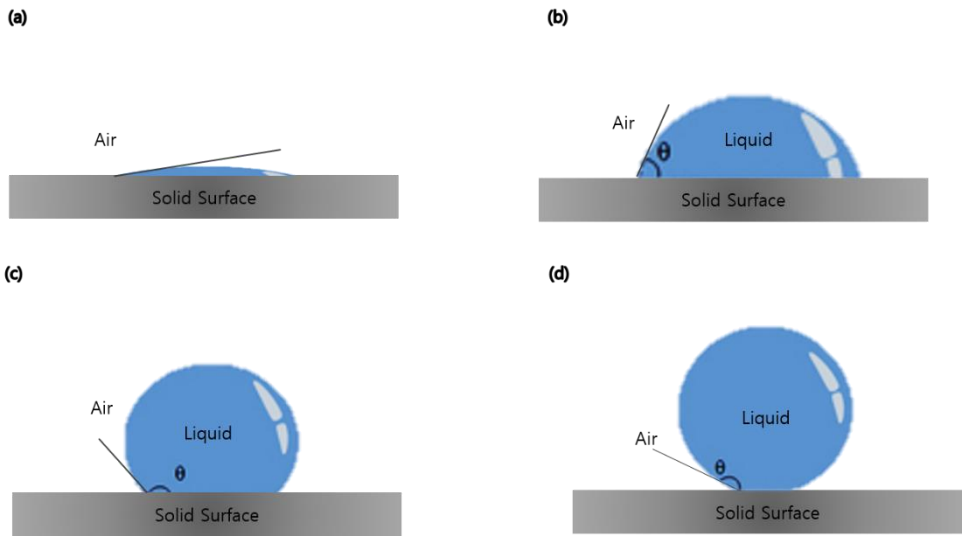

Figure 3. Four classes of surface wettability, their characteristic static contact angles. (a) Superhydrophilic CA<10°, (b) Hydrophilic 10°<CA<90°, (c) Hydrophobic CA 90–150°, and (d) Superhydrophoic CA>150°.

In 1805, Young firstly proposed the theory of static contact angle (θ) of a liquid droplet on a flat surface by analyzing the forces acting on droplets surrounded by air [16]. The droplets form a three-phase contact line where solid-liquid, solid–vapor, and liquid–vapor interfaces meet. Forces created by the surface tensions at each interface are pulling droplet in solid plane and define its shape. According to the Young's equation, the cosine of the water contact angle in the equilibrium state (θ_Y) is directly proportional to the difference of the interfacial forces per unit length of solid–vapor (γ_{SV}) and solid–liquid interfaces (γ_{SL}), and inversely proportional to the interfacial force of the liquid–vapor (γ_{LV}) interface. Young expressed the contact angle θ_Y of a water droplet on a flat surface by the following equation:

$$\cos\theta_Y = \frac{\gamma_{SV}-\gamma_{SL}}{\gamma_{LV}} \quad (1)$$

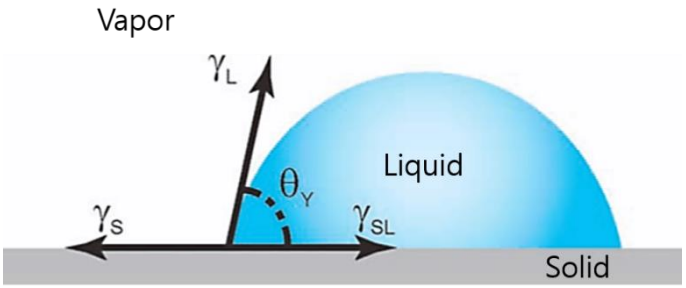

Figure 4. Schematic diagram of static contact angle for liquid droplet on smooth solid surface.

This relationship is depicted in **Figure 4**. It can be seen from the figure and the equation 1 that the static WCA can be increased by lowering the surface tension of a solid material, since the surface tensions of water and surrounding medium (usually air) are fixed and defined. The chemical groups with low surface energies can be ordered as $\gamma_{CH_2} > \gamma_{CH_3} > \gamma_{CF_2} > \gamma_{CH_2F} > \gamma_{CF_3}$. [17] The lowest surface energy of 6.7 mJ/m^2 was obtained for regularly aligned closest-hexagonal-packed CF_3 groups [18]. However, the static WCA of a smooth surface produced from this material can reach only 119° [19], which is far away from the requirements of superhydrophobic surfaces.

Wenzel [20] found that the surface roughness could significantly change the water contact angle values on surface. He assumed that water follows all topological variations of a surface as shown in **Figure 5(a)**, thus increasing the water–liquid interface. Wenzel's assumption is also called homogeneous wetting. Based on this assumption, the author derived an equation that relates surface roughness (r) and Young's contact angle (θ_Y) to the actual water contact angle on a rough surface (θ_w). [21]

$$\cos\theta_w = r\cos\theta_Y \tag{2}$$

The roughness factor r is the ratio of the water-solid contact area to the area of geometrical projection of water-solid interface (excluding surface topology) [22]. If the surface roughness factor is unity, then equation (2) transforms into equation (1). Since water droplets penetrate into small cavities on the surface, the surface roughness factor is always greater than unity, leading to an increase in contact angle

for hydrophobic surfaces and a decrease in contact angle for hydrophilic surfaces.

Later Cassie and Baxter [23] proposed another model to explain the effect of roughness on droplet behavior on a surface. In contrast to Wenzel, they assumed heterogeneous wetting when air is entrapped by water in surface cavities as shown in **Figure 5(b)**. In such case, the contact area between water and the solid is minimized, and the area between water and air is maximized, thus forcing water to form spherical droplets. In addition, roughness of wet areas also influences the contact angle, and in general, Cassie's equation can be described as:

$$\cos\theta_C = f\cos\theta_Y + f - 1 \tag{3}$$

where f is the ratio of the solid–liquid contact area to the area of geometrical projection of the water droplet [24]. Therefore, when f decreases as more air is trapped, surface roughness and contact angle greatly increase.

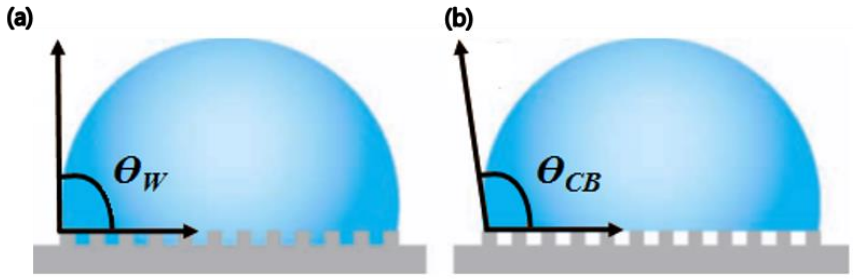

Figure 5. Water droplets on Wenzel state solid surface (a) and Cassie-Baxter state solid surface (b).

Both the Wenzel and Cassie–Baxter models describe how the contact angle increases with an increase in surface roughness. However, these models do not consider the dynamic behavior of a droplet when it moves on a surface. Both Wenzel and Cassie–Baxter models show a high contact angle on rough hydrophobic surfaces **in Figure 5**; however, the results of contact-angle hysteresis are entirely different in both cases.

In the Wenzel model, the liquid phase permeates all cavities, voids, and pours on the surface of the solids, and is strongly attached to the surface, resulting in relatively high-contact angle values where a higher force is expected to move the attached droplet from the surface. According to the Wenzel model hypothesis, an increase in surface roughness also increases the surface area, which leads to enhanced hydrophobicity, since water permeates cavities on the rough surface leading to better pinning (or stationary droplets), and such a surface shows a high hysteresis as well.

In the Cassie–Baxter model, the contact between water and the solid is fairly small, resulting in lower hysteresis; so the droplet moves at a small tilt angle. Consequently, this model is most likely the better way of creating superhydrophobic surfaces for a better self-cleaning option. In the Wenzel model, the surface with the higher roughness increases both contact angle and hysteresis. Nevertheless, when the roughness factor increases to a certain value, water droplets cannot occupy all voids and cavities on the surface, and subsequently a transition from the Wenzel model to the Cassie–Baxter model occurs, during which some air packets are trapped underneath the liquid droplet. In this case, when roughness is

further increased for a higher contact angle, the hysteresis can be significantly reduced as well. The dynamic behavior of a water droplet on an inclined surface is shown in **Figure 6**. A water droplet on a tilted surface has a different contact angle on each side of the drop.

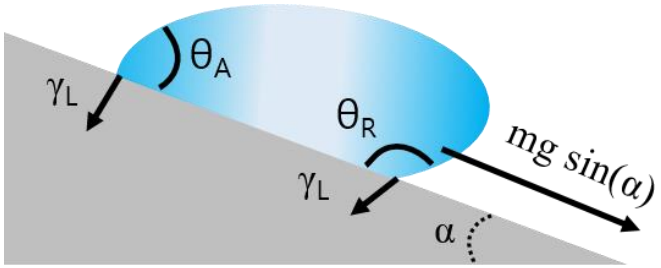

Figure 6. Schematic view of water droplet on a tilted surface with advancing angle, receding angle and tilting angle.

The angle in front of the droplet motion is called the advancing angle (θ_A), while the angle on the other side of the drop is called the receding angle (θ_R), and the difference between the two angles ($H = \theta_R - \theta_A$) is called the contact angle hysteresis. Hysteresis creates force (F) required to move the droplet:

$$F = \gamma_{LV}(\cos\theta_{R(min)} - \cos\theta_{A(max)}) \quad (4)$$

where γ_{LV} is the interfacial energy of the liquid–vapor interface, and $\cos\theta_{R(min)} - \cos\theta_{A(max)}$ is the contact angle hysteresis.

On the inclined surface, the force that interacts against the pinning force is created by gravity and depends on the tilt angle. Therefore, the critical tilt angle (θ_C), that is, required to initiate droplet motion depends on the contact angle hysteresis and can be derived from the next equation:

$$\frac{mgSig\theta_C}{d} \geq \gamma_{LV}(\cos\theta_{R(min)} - \cos\theta_{A(max)}) \quad (5)$$

where m is the weight of the droplet, g is the acceleration due to gravity, and d is diameter of the droplet. One can easily observe from equation (5) that the reduction in contact-angle hysteresis causes a reduction in the critical tilt angle, which may greatly affect the self-cleaning property. Fundamental studies discussed previously clearly show that the combination of proper surface chemistry and topology can be utilized to produce surfaces with superhydrophobic and self-cleaning properties. Fundamentally, significant progress in the classical models as well as experimental research have revealed that the morphological roughness with a micro- and nano-sized structures plays an important role in realization of highly hydrophobic surfaces.

The validity of the Wenzel's equation and Cassie's equation has been investigated for many years. There are still many controversies on the two equations. The complexity of the problem also comes from the contact angle hysteresis. The effective contact angle of liquid drops on rough or inhomogeneous surfaces could take a range of values, depending on the history of the liquid drop. It is believed that the multiple effective contact angles are related to the local minimums of the free energy of the system, which cannot be described by Eqs. 2 or 3. The behavior

of the solution for a periodically patterned surface is studied in the limit of the small ε period, by Xianmin Xu, etc [25]. They assumed that the bottom of the superhydrophobic solid surface is composed of periodically patterned two materials, as can be shown in **Figure 7**. The contact angle function in periodic pattern in both x and y with a ε period can be provided as follows;

$$\cos\theta_Y(x,y) = \begin{cases} \theta_{Y1}, \text{if } (x,y) \text{ is in material 1;} \\ \theta_{Y2}, \text{if } (x,y) \text{ is in material 2.} \end{cases} \quad (6)$$

Then, they derived a modified Cassie's equation for chemically rough surfaces from the Young-Laplace equation and the Young equation with a homogenization approach. The derivation reveals that effective contact angle is a local average of the static contact angle along the contact line which describes all possible equilibrium states including the local minimum of the free energy of the system. The usual Cassie's state which corresponds to the global minimum is only a special case. The modified Cassie's equation is given by

$$\cos\theta_a = \frac{1}{\varepsilon}\int_0^{\varepsilon} \cos\theta_Y(x,y)|_{x=\varepsilon u(\frac{y}{\varepsilon},0)}\, dy \quad (7)$$

Then, θ_a is the apparent contact angle. The right hand side term is the integral average of the local static contact angle along the contact line in one period of y. The modified Cassie equation can be used to describe contact angle hysteresis while the usual Cassie's state, which only corresponds to the global minimum of the total energy of the system, is unable to explain the contact angle hysteresis phenomena.

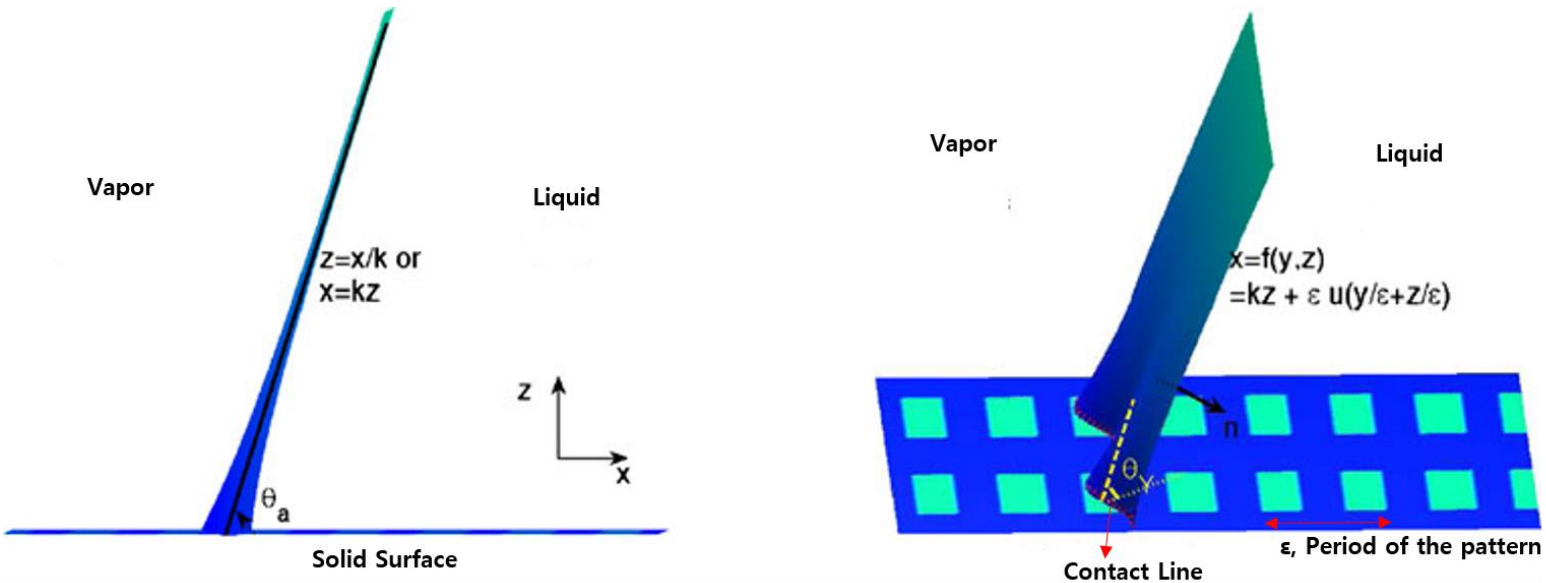

Figure 7. Geometry properties of the liquid–gas interface (a) The apparent contact angle (b) The unit normal to the surface and the Young's angle [25].

Ⅱ. Superhydrophobic Surfaces on Cotton Fabrics

2.1 Introduction

Water repellency and soil resistivity have been the most desirable textile properties for consumers. Surface properties of textile manufactures have been considerably investigated and improved for many decades. A fabric surface with a water contact angle higher than 150° is considered to be a material having a practically non-wettable superhydrophobic. Textiles or membranes are generally believed to be rough substrates with reentrant curvatures and controllable diameter or spacing of fibers that are suitable for the achievement of super-repellent ability [26]. So far, superhydrophobic textile materials have been successfully developed by different technical approaches.

Among the textiles, cotton fabric is the most abundantly and widely used natural fiber cloth today and has always been the principal fiber for clothing due to its attractive characteristics such as softness, comfort, high resistance to heat, and high resistance to alkaline. Despite the excellent properties of cotton fibers, some inherent features such as being hydrophilic, poor resistance to UV light (color yellowing), impotent antimicrobial activity, have confined their wider applications, especially in some high-tech fields for self-cleaning, medicine, personal healthcare, and flexible multifunctional textile.

The cotton is composed of almost pure cellulose fiber of hydrophilic property. Because the cellulose fiber is a linear polysaccharide polymer with many hydroxyl groups, as shown in **Figure 8**, common cotton fabrics are hydrophilic in nature. Its high absorbency because of the abundant hydroxyl groups on cotton diminishes the stain-resistance and water repellency of cotton textiles.

If the cotton surface is extremely repellent to water, it would have various commercial, military, and advanced multifunctional applications from self-cleaning, anti-fouling, stain-free and spill-resistant protective wear [27, 28] to anti-icing, liquid manipulation, fluidic drag reduction, water collection, selective transportation of microdroplets. [29-32] Therefore, the work was done for impartment the extremely water-repellent properties i.e., superhydrophobicity a to cotton fabrics.

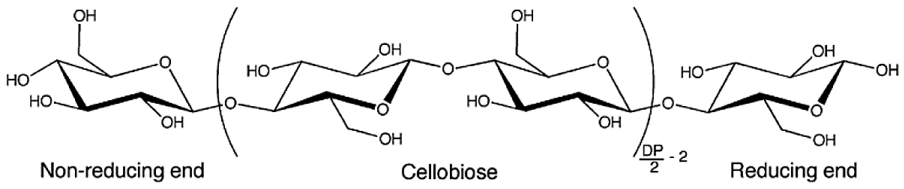

Figure 8. Chemical structure of cellulose fiber constituting the cotton textile.

Based on the principles of superhydrophobicity it is now clear that the effects of low surface energy and hierarchical roughness topography are required. Chemicals with low surface energy, such as fluorine- and silicone- containing polymers as well as hydrocarbons can be applied to cotton fibers by grafting, adsorption, chemical vapor deposition, etc. On the other hand, the creation of hierarchical roughness may be the more demanding step toward superhydrophobic cotton textile.

The most common techniques to construct rough coatings for the superhydrophobic fabric include various dip-coating methods, wet chemical etching, chemical bath deposition, electro-assistant deposition (electrophoretic deposition, electro-spinning), spray-coating, chemical vapor deposition, and plasma processing techniques. The summary of most common synthesis techniques for superhydrophobic coatings on cotton substrates is listed in **Table 1**.

So far, a number of studies have been reported on the superhydrophobic surfaces of the cotton textiles. Gold particles have been incorporated into cotton fabrics to develop a micro- as well as nano-size surface morphology by Wang et al. [33]. Chemical vapor deposition (CVD) is a typical dry technique enable tuning of chemical and physical fine structure to be deposited onto a substrate in the form of nonvolatile film via the reaction of gaseous reactants. Zhou et al. introduced the incorporation of polyaniline and fluorinated alkyl silane to the cotton fabric via a facile vapor phase deposition process [34]. The treated fabric surface possessed both superhydrophobicity with the water contact angle of 156° and superoleophilicity with the oil contact angle of 0°.

Table 1. Common techniques to construct superhydrophobic textiles and general characteristics of the different techniques and surfaces.

Method	Roughness Formation	Time-Scale and Requirement	Properties
Dip-coating	Nanoparticle Coating	Slow	Mechanical and environmental stability
Wet Chemical Etching	Growth of nano-structures by etching	Rapid/slow	Excellent resistance to washing, abrasion
Chemical Bath Disposition	Nanoparticle film deposition	Slow and temperature requirement	Moderate durability
Electrophoretic Deposition	Nanoparticle coating	Rapid and conductive substrate requirement	Chemical stability, highly transparent
Electrospinning	Nanofibers by electrospinning	Slow and solvent requirement	Porous membrane
Spray-coating	Micro/nanostructures by spraying	Rapid and scalable under ambient conditions	Moderate stability, easy reparability
Chemical Vapor Deposition	Growth of nano structures by polymerization	Slow and need heating	Separation of oils or organic contaminates from water
Plasma Etching Process	Growth of nanostructures by etching	Moderate and require specific equipment	Self-cleaning

The dry plasma etching processing is important for the rough structure construction on some specific cellulose fiber. Plasma surface treatment of cotton fabrics was carried out in a hexafluoropropene (C_3F_6) atmosphere under different experimental conditions by Shen Li et al. [35]. The hydrophobicity and tensile strength were considerably improved after plasma treatment. However, these expensive nanomaterials and costly instruments are not necessary for preparing superhydrophobic cotton and may limit their practical applications.

Superhydrophobic textiles with micro/nano-scale binary structure surfaces can be developed using nanoparticles such as silica, TiO_2, CNT, ZnO, etc., in various ways. Zhao et al. [36] used the layer by layer (LBL) assembly method on cotton fabrics to give roughness using polyelectrolyte/silica nanoparticle multilayers and post-treating with fluoroalkylsilane to develop superhydrophobic textiles with a sliding angle (SA) of 10° even after ten washes. In developing superhydrophobic textile fabrics, TiO_2 nano aggregates were also used to create a binary roughness on the fabric surface by a sol-gel method with post treatment using stearic acid and 1H,1H,2H,2H-perfluorodecyltrichlorosilane (PFTDS) to lower surface energy by Xue et al. [37]. Furthermore, TiO_2 crystallization and aggregation exhibited UV blocking abilities by scattering light, thus showing the possibility of developing multi-functional fabrics. Although most reports demonstrated that super-antiwetting surfaces with special wettability could been fabricated via a single method or process to successfully change sole surface structure/component or both of them simultaneously, dual/multiple processes are required to realize structural and chemical requirements in some specific cases. Therefore, more simple

fabrication process has been requested.

Spray-coating is a facile, rapid and versatile way to build the hierarchal binary roughness structures on the surface by nanoparticle deposition. It can be used to coat a layer of low surface energy polymer on all kinds of substrates. For example, Yang et al. [38] fabricated superhydrophobic/superoleophilic epoxy/attapulgite nanocomposite coatings on the stainless steel meshes by a simple spray-coating process. The authors demonstrated the coated mesh maintained highly superhydrophobic property after being treated in various harsh conditions, including mechanical scratch, high temperature, humid atmospheres, and corrosive substance.

In this report, the extremely water repellent and transparent surfaces were fabricated on cotton fabrics coated with the hydrophobized silica nanoparticles by spray-coating. The hydrophobized silica nanoparticles were dispersed in alcohol solvents (1-propanol, ethanol, and methanol) and the effect of the three types of alcohols on superhydrophobicity of the cotton fabric substrates was investigated. To confirm the superhydrophobicity, the contact angles as well as contact angle hysteresis were measured and compared.

2.2 Experimental Section

2.2.1 Materials

A 25 cm^2 square piece of cotton textile (Taipyung Textile Co.) was cleaned with water and ethanol to remove impurities. The characteristics of fabric are shown **Table 2**. Fumed silica nanoparticle (Aerosil) having an average diameter of 16 nm was used for hierarchical structure development. To transform the hydrophilic silica nanoparticles into the hydrophobic ones, dodecyltrichlorosilane (DTS) (Aldrich) as a silane coupling agent was used. Molecular formula of the DTS is $C_{12}H_{25}Cl_3Si$ and it is well known as very hydrophobic material (**Figure 9**). Toluene and methyl alcohol, ethyl alcohol (Samchun Chemicals), propyl alcohol (JUNSEI) were used without further purification.

Table 2. Characteristic of cotton textile.

Cotton	Value
Yarn count	60'S
Weight (g/m^2)	60.5
Density (warp x weft)	101 x 85
Thickness (mm)	0.132
Weave type	Plain structure

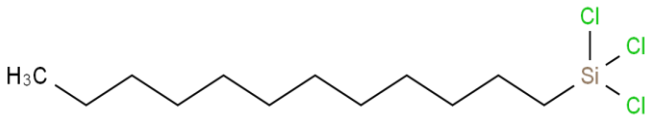

Figure 9. Molecular structure of dodecyltrichlorosilane presenting hydrophobic property.

2.2.2 Superhydrophobic treatment

1g of silica nanoparticles were added to 20 mL of toluene. After dispersion, 1 mL of dodecyltrichlorosilane, as a silane coupling agent, was dropwise added to the solution. Thereafter, the reaction vessel was stirred for 2 hours at room temperature. The purpose of this treatment is the adhesion of dodecyltrichloro groups on silica nanoparticles surface and making them hydrophobic. All chlorosilanes react with hydroxide of silica to produce hydrogen chloride. The remaining hydroxyl group bonds to the silicon, initially forming a silol group (analogous to alcohol). In general, this will eventually bond to a solid oxide surface or react with another chlorosilane or silol molecule. In the latter cases, the oxygen atom forms a link between two silicon atoms, analogous to the ether linkage in organic chemicals, and identical to the bonding in silicon dioxide. The hydrophobic silica coated with dodecyl triethoxysilane would be generated as scheme presented in **Figure 10**. The solution was filtered, dried under vacuum at 323 K for 8 hours and triturated using a pestle and a mortar.

2.2.3 Air Spray coating

0.3g of trichlorododecylsilane treated silica nanoparticles were added to 15mL of methyl alcohol, ethyl alcohol, and propyl alcohol. The solution was treated using a bath sonicator for 30 min and was stirred vigorously for another 1 h to obtain a stable and homogeneous suspension. The mixtures were manually sprayed over cotton textiles from 20cm away using an air spray gun (Anest Iwata). The resulting coated samples were dried at room temperature for 24 h.

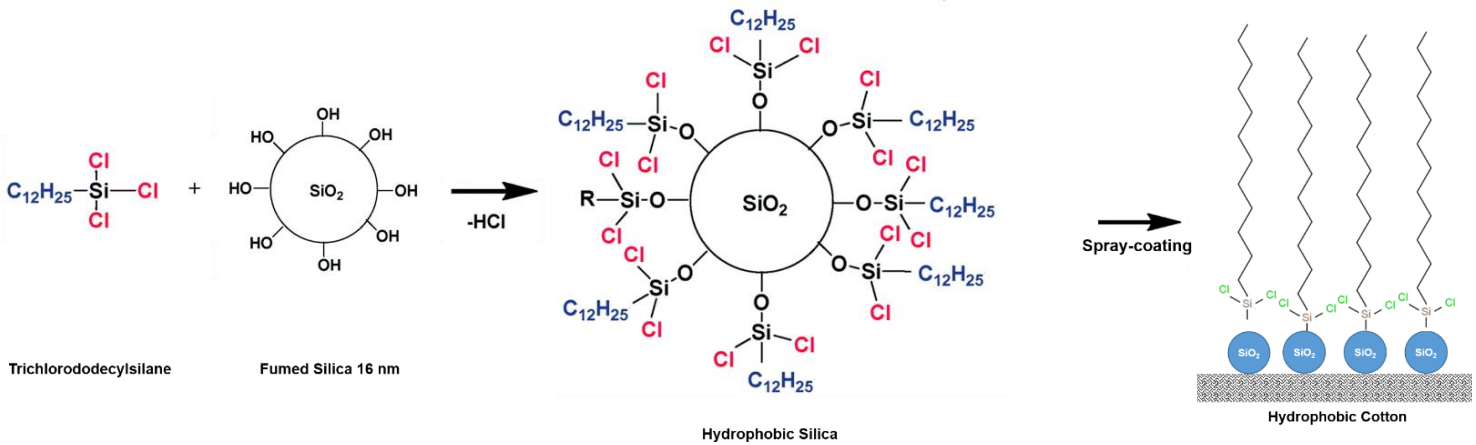

Figure 10. Schematic view of hydrophobic treatment on fumed silica nanoparticles with dodecyltrichlorosilane material.

2.2.4 Characterization

The surface morphologies of the superhydrophobic treated fabrics were examined by scanning electron microscopy (JSM-7600F, JEOL). The dispersion of silica nanoparticles in the three different solvent was determined using a UV–vis spectrophotometer (Hitachi U-2800) operating at 600 nm. The formation of –Si–O–Si– linkages was confirmed by NMR spectroscopy (Bruker AVANCE-II 500 MHz). For the measurements, the pristine silica and hydrophobic treated silica nanoparticles were dissolved in $CDCl_3$ and scanned 16 times. The particle size distributions of methyl alcohol, ethyl alcohol, and propyl alcohol containing the superhydrophobic treated silica nanoparticles were measured using Particle size analyzer (Nanotrac, Microtrac^{TM}). The averages of 3 different measurements of each were recorded.

2.2.5 Water contact angle and hysteresis

The wettability of the superhydrophobic treated cotton textile was evaluated by water contact angles and hysteresis of water droplets on the cotton textiles using a contact angle meter (SmartDrop, Femtofab). For the contact angles measurement, water droplets with a volume of 3 μL were dispensed using micropipette onto the fabric surface. The average contact angle was obtained by measuring at four different positions of the sample. For the contact angle hysteresis analysis, the advancing and receding angles were obtained using the captive method, as shown in **Figure 11**.

While a water droplet of 5.0 μL were suspended to the needle, it spurted out the additional water to 7.5 μL and the advancing contact angle (θ_a) was measured at three different volumes. The receding angle measurement was followed after reducing the water volume to 5.0 μL. The three receding contact angles (θ_b) were measured while the additional suctions to 2.5 μL.

The hysteresis was calculated as the difference between the averaged values of three advancing and receding angles, respectively ($\Delta\theta = \theta_a - \theta_b$). To identify the transparency and visibility of the silica nanoparticle coated cotton substrates, pictures of a drop of water on it were taken.

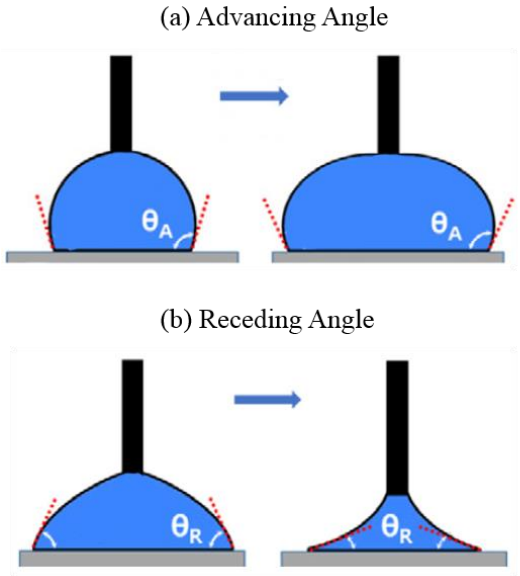

Figure 11. Schematic view of the captive method for hysteresis measurement. Advancing contact angles measurement (a) and receding contact angles measurement (b).

2.2.6 Washing durability

To determine the washing durability of the superhydrophobic cotton fabrics treated with different alcohol, the samples were agitated by a magnetic stirrer at 300 rpm for 30 min in the absence and in the presence of the detergent. As a detergent, 1 % of Persil® (Henkel) composed of anionic surfactant was used. After washing treatment, the fabrics were dried at room temperature for 24 h. The average values of 3 different measurement of contact angle and sliding angles of washed cotton fabrics are recorded. For the sliding angle measurements, a water droplet of 5.0 μL was placed at different positions on the cotton fabrics. The tilting angle of the stage on which the cotton textiles lie was increased by 0.1°, and the angle at which a water droplet rolls off of a 2 cm distance or greater on the cotton fabrics was recorded and referred as sliding angle.

2.3 Results and Discussion

As shown in **Figure 10**, silica nanoparticles were modified with dodecyltrichloro silane to make it superhydrophobic. Solid state Si-NMR spectra and XPS spectrum of the samples were used to confirm chemical bond formation by reaction of trichloro(alkyl)silane with surface hydroxyl groups (silanols) of the silica nanoparticle.

The XPS spectrum of treated silica nanoparticles in **Figure 12** shows the presence of Si and O from the fumed silica, C and Cl from the alkylsilane agent. That is, after the treatment, the trichloro(alkyl)silane group have been successfully attached to the fumed silica nanoparticles. The Si-NMR spectra of the samples are provided in **Figure 13**. The spectra of the fumed silica nanoparticles showed the rough peak at 110 ppm with a shoulder peak at 100 ppm, which was assigned to the connecting SiO_4 tetrahedra, where the 1 and 2 signals correspond to silicon atoms bonded to four and three oxygen atoms, respectively

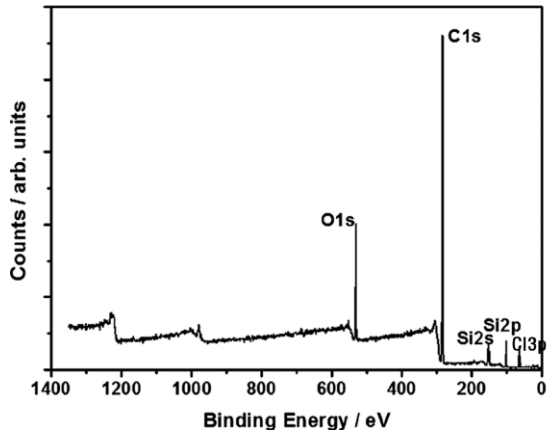

Figure 12. X-ray photoelectron spectroscopy results of (a) the fumed silica and (b) modified silica nanoparticles with dodecyltrichlorosilane.

On the other hand, the spectra of the modified silica nanoparticles exhibited more strong peak at 100 and 110 ppm, and two other well-resolved peaks at 57 ppm and 68 ppm were assigned to the general alkylsiloxane structures $(HO)(R)Si(OSi)_2$ [isolated silanol, 4] and $(R)Si(OSi)_3$ [siloxane, 3], where R = alkyl. The presence of 3and 4 peaks in the spectra indicates that the network structures exhibit two and three cross-links with silanols of the silica nanoparticles.

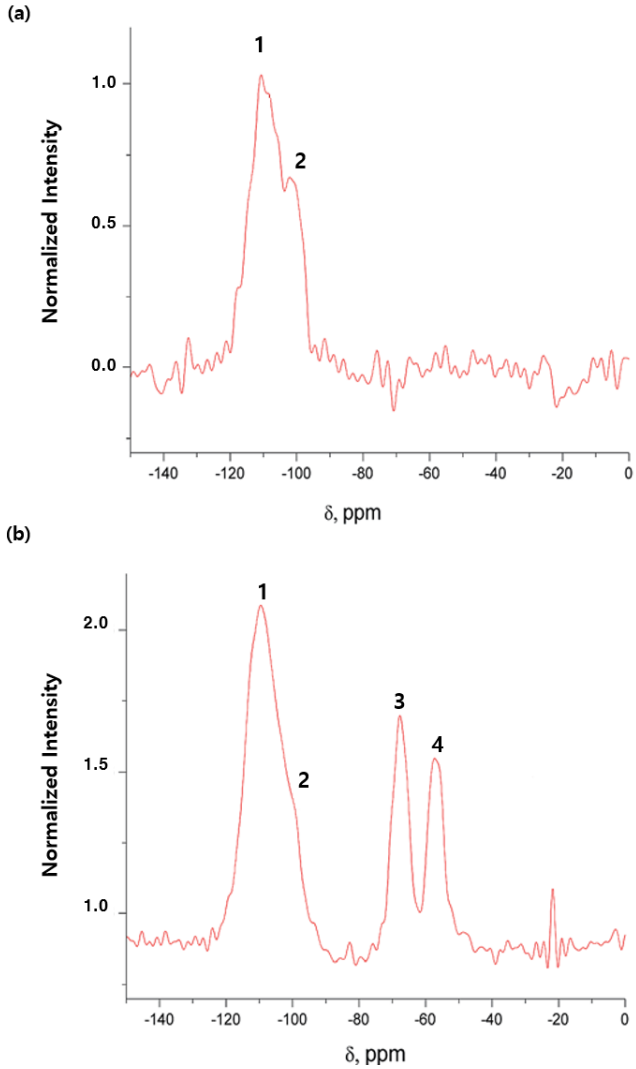

Figure 13. NMR spectra of (a) the fumed silica and (b) modified silica nanoparticles with dodecyltrichlorosilane.

In order to convert the hydrophilic cotton textiles into the extremely water-repellent hydrophobic fabrics, the trichlorododecylsilane treated silica nanoparticles were spray-coated on the cotton fabrics using the alcohol solvents. Three types of the alcohol solvent were used to confirm the effect on the surface roughness, the superhydrophobicity of the coated cotton fabrics. The shorter the chain length of the alcohol's hydrocarbon had, the stronger the superhydrophobicity of the coated cotton fabric became.

The water droplet on each cotton fabrics can be seen in **Figure 14**. As mentioned in other literatures, due to the protrudent fibers from the cotton surface, it is difficult to determine the baseline of the water droplet, which may in turn lead to underestimation of the contact angles from other conventional device using 3 points near the contact line. Contact angle data near the contact angle is vulnerable to optical distortion and interfacial distortion. However, in this study, the SmartDrop measurement system estimated the rate of change of curvature of the free surfaces, calculated the value of the distorted surfaces and provided the more accurate liquid droplet information without any loss of contact angles. It is known that the contact angle of a water droplet is more accurately calculated by the influence of gravity and the surface tension of a droplet by applying the interface analysis algorithm, Bashforth-Adams equation applied to the equipment.

$$\gamma_{lv}\left\{Z^{"}/(1+z'^{2})^{\frac{3}{2}}+z'/[x(1+z'^{2})^{\frac{1}{2}}]\right\}=\frac{2\gamma_{lv}}{\mathrm{b}}+\Delta\rho gz \qquad (8)$$

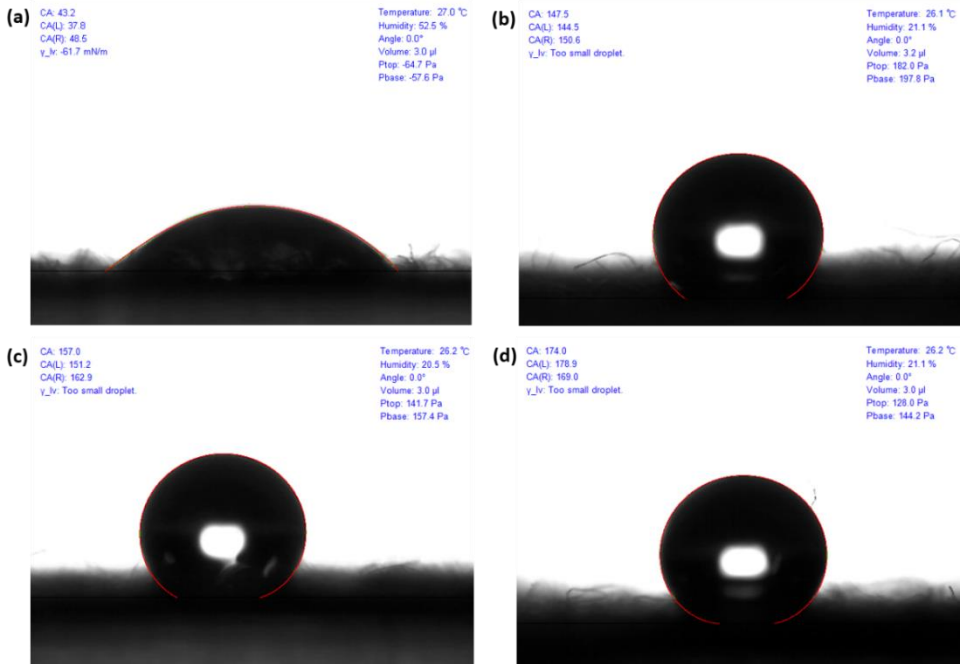

Figure 14. Captured images of the water droplets (3 µL) placed on the cotton fabrics showing the CAs and the specifications. (a) Pristine cotton fabric, (b) cotton fabric coated in 1-propanol (c) cotton fabric coated in ethanol (d) cotton fabric coated in methanol.

Based on the red lines that present the real droplets of water on the cotton fabrics, the water contact angles were calculated. In case of pristine cotton, most of the water droplet were absorbed into the hydrophilic cotton surface. However, droplets of water onto the cotton fabrics coated by hydrophobized silica nanoparticles were not absorbed at all and looks spherical. In addition, as the chain length of the alcohol's hydrocarbon was shorter, it is getting closer to the perfect sphere and the contact area are reduced. This image results are well consistent with the average contact angle values of pristine and the cotton fabrics coated with silica nanoparticles in 1-propanol, ethanol, and methanol. **Figure 15** shows the contact angle values, i.e., the average ones of the left and the right angles.

As expected, the pristine cotton fabric shows the hydrophilic property. The contact angles of pristine cotton are about 40°. However, all of the coated cotton fabrics showed the significantly increased water contact angles compared with the uncoated one. The average contact angle values of the cotton fabric coated with silica nanoparticles in 1-propanol, ethanol, and methanol are 147.8°, 158°, and 176° respectively. This means that the spray-coatings of the hydrophobized silica nanoparticles converted the hydrophilic cotton textiles into the hydrophobic ones. In addition, it is shown that the contact angles coated in ethanol were higher than that in 1-propanol and the contact angles in methanol showed more increased values than that in ethanol. In particular, the contact angles of the cotton fabrics coated in methanol show the high contact angles larger than 170°.

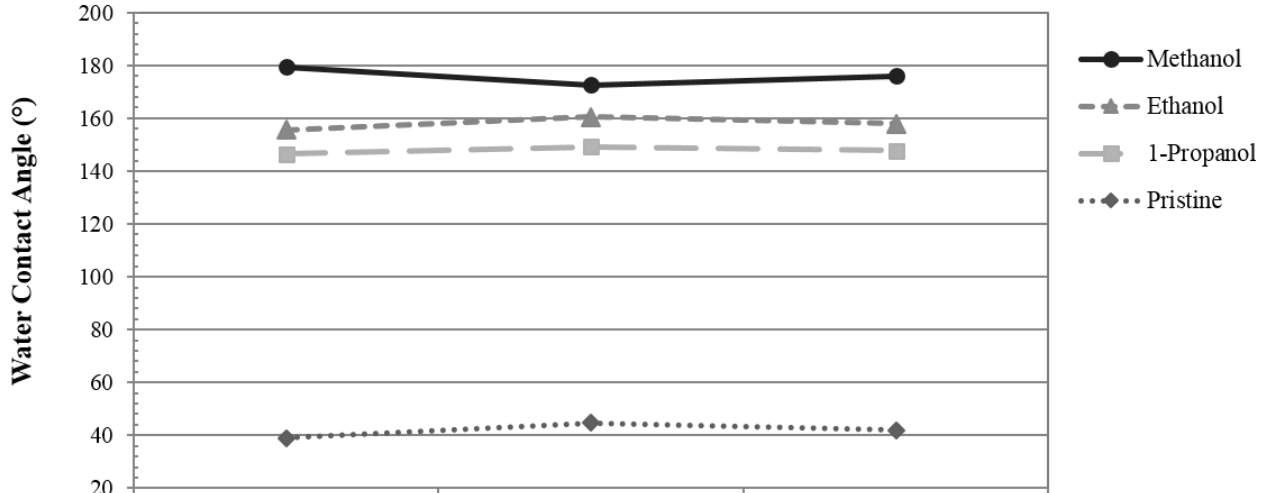

	Left Angle	Right Angle	Contact Angle
Methanol	179.4	172.6	176
Ethanol	155.6	160.4	158
1-Propanol	146.4	149.2	147.8
Pristine	38.9	44.8	41.9

Figure 15. Water contact angles of pristine and the cotton fabrics coated with silica nanoparticles in 1-propanol, ethanol, and methanol.

In addition, the protruding cotton fibers made it difficult to evaluate the roll-off angles, sliding angles, or hysteresis using the conventional methods that measure the values by tilting the stage on which the samples are placed. Especially, in the case of the superhydrophobic surfaces that have the extremely high water repellency, the water droplet tends to bounce out easily. In this study, the captive method, in which water droplets are suspended, emits droplets while measuring the advancing contact angles and sucks them while determining the receding contact angles, was applied to the analysis system and the accurate results were obtained in **Figs 16-18**.

When the length of the hydrocarbon of the alcohol solvent is decreased, the water droplets remained the more spherical shape and the smaller difference between the advancing and receding angles. In **Figure 19**, it can be distinguished that the more detailed hysteresis differences according to the alcohol solvent. The hysteresis is diminished as the length of the hydrocarbon of the alcohol solvent is decreased. Especially, the difference between the advancing and receding angles lower than 10° was obtained only from the methanol solvent (**Table 3**). The result values from the ethanol and the 1-propanol were higher than 10° and the hydrophobic tendency is agreement well with the contact angle results. Typically, hierarchically structured surfaces have the significantly low solid-liquid contact area and this results in the highly low contact angle hysteresis. Therefore, it can be concluded that the coated cotton fabrics in methanol showed the contact angles higher than 150° and the hysteresis lower than 10° can be considered the only superhydrophobic surfaces.

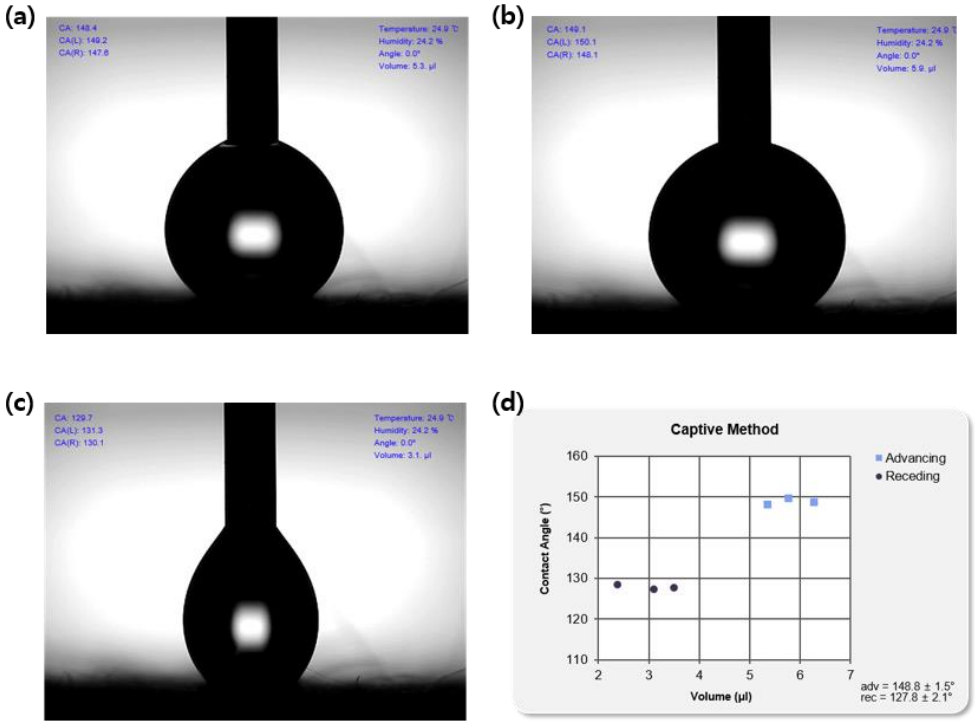

Figure 16. Photographs of captive method for hysteresis (a) at start point, (b) advancing point, and (c) receding point of the cotton fabrics coated with silica nanoparticles in 1-propanol. Graph the advancing and receding angle values (d).

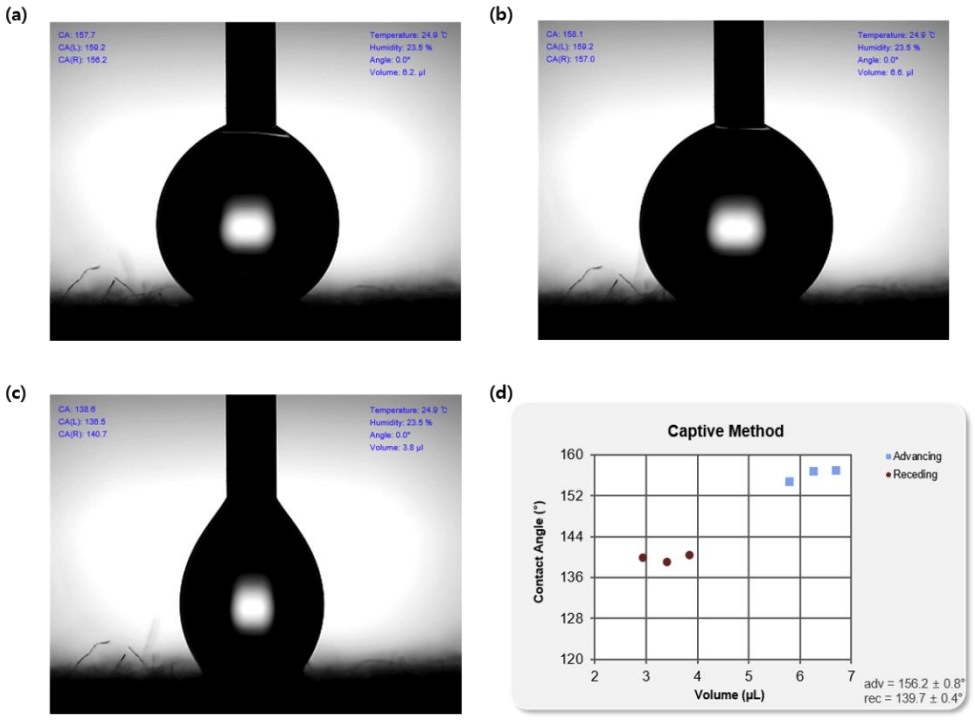

Figure 17. Photographs of captive method for hysteresis (a) at start point, (b) advancing point, and (c) receding point of the cotton fabrics coated with silica nanoparticles in ethanol. Graph the advancing and receding angle values (d).

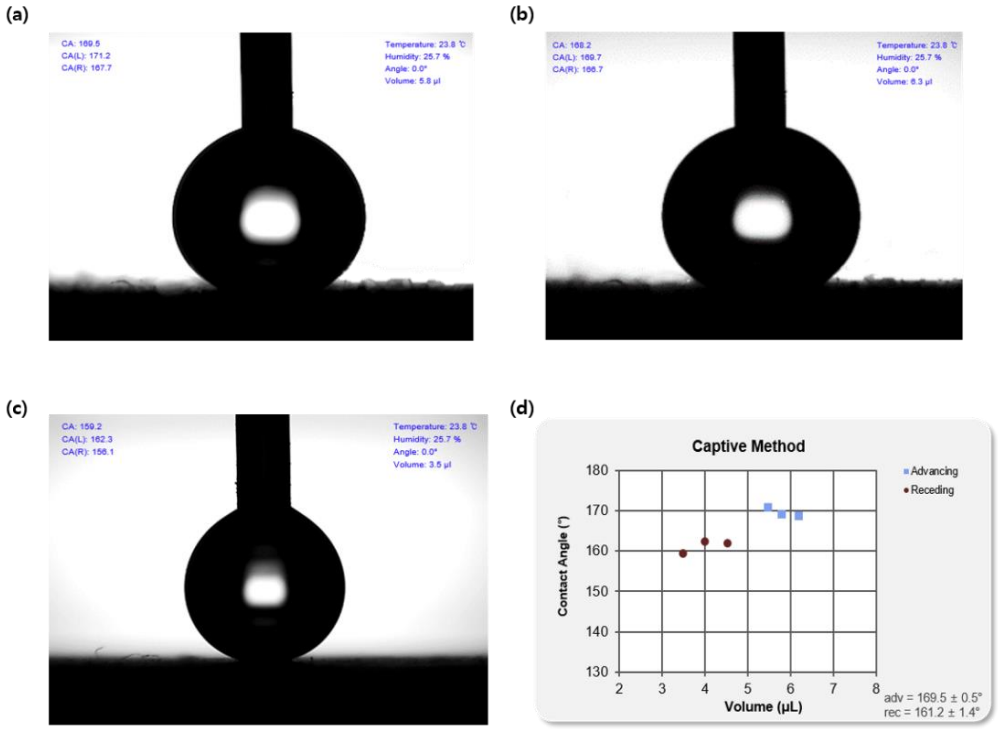

Figure 18. Photographs of captive method for hysteresis (a) at start point, (b) advancing point, and (c) receding point of the cotton fabrics coated with silica nanoparticles in methanol. Graph the advancing and receding angle values (d).

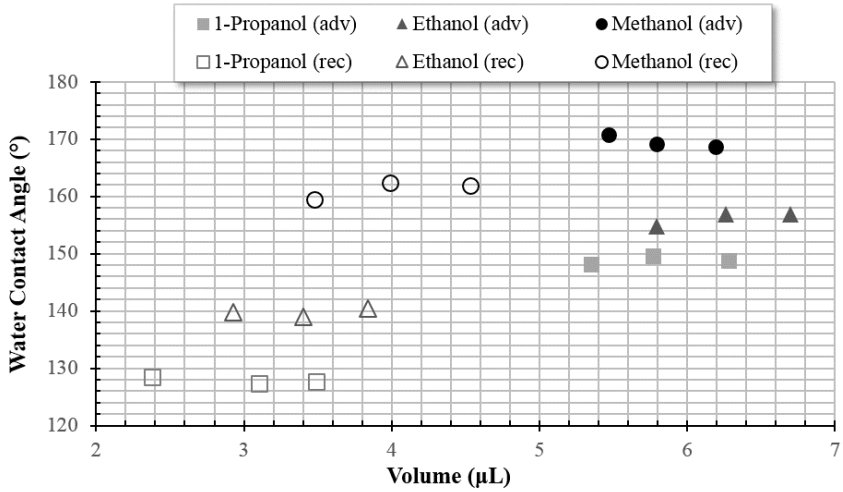

Figure 19. Advancing and receding contact angles of the cotton fabrics coated with silica nanoparticles in 1-propanol, ethanol, and methanol, respectively measured by the captive method.

Table 3. The averaged advancing and receding angles, their difference, hysteresis the cotton fabrics coated with silica nanoparticles in 1-propanol, ethanol, and methanol.

Alcohol	Advancing/deg	Receding/deg	Hysteresis/deg
1-Propanol	146.37	126.21	20.16
Ethanol	156.21	139.74	16.47
Methanol	169.53	161.24	8.3

It can be concluded that the water contact angles increased as the length of hydrocarbon chain of alcohol solvent decreased. It is reasonable that hydrophobic silica nanoparticles with dodecyl groups tend to aggregate in the less hydrophobic alcohols.

The wettability of surfaces is governed by two major factors. One is the chemical composition of the solid surface and the liquid, and the other is the geometry of the solid surfaces. As the surface energy of the hydrophobized silica nanoparticles would be the same, the type of the solvent would have affected the surface roughness of the cotton fabrics coated with silica nanoparticles. In order to confirm the effect of the alcohol on the surface morphology, SEM images of silica nanoparticles coated cotton fabric in 1-propanol, ethanol, and methanol were measured. The pristine cotton textile presents a highly textured micro-scale fiber with a typical smooth surface in **Figures 20 (a) and (b)**. In low magnification SEM images of treated cotton fabrics, it can be seen that the silica nanoparticles cover the cotton fibers not uniformly and are aggregated partially. In addition, there are the more silica nanoparticles aggregates in methanol than others. In high magnification images, the morphological differences can be more clearly visible.

Generally, superhydrophobicity tends to be exhibited when hydrophobic surfaces have hierarchical roughness, both nanometer- and micrometer-sized roughness. As shown in **Figure 20**, the nano-sized silica nanoparticles are well developed and form the rough structures in methanol. Whereas, the silica nanoparticles in 1-propanol and ethanol are relatively vague. Based on these SEM images, it is reasonable that the hierarchically rough surface was well formed in methanol and

it induced the superhydrophobicity of the cotton fabric.

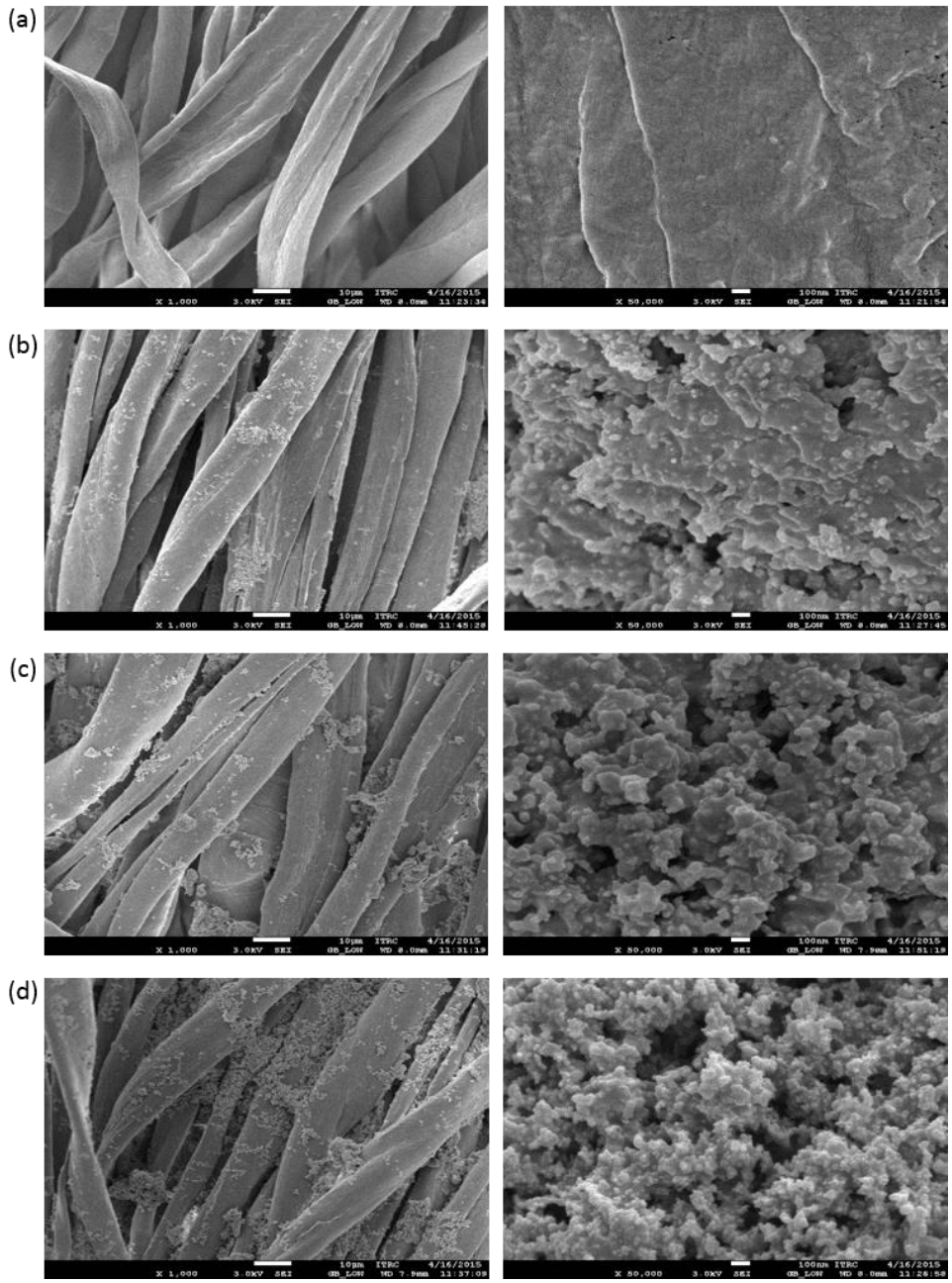

Figure 20. SEM images of SiO_2 NPs-covered cotton fabrics. The images on the left are low-magnification ones and that on the light are high-magnification ones. (a) pristine cotton fibers, (b) the cotton fibers coated in 1-propanol, (c) the cotton fibers coated in ethanol, (d) the cotton fibers coated in methanol.

In contrast, the silica nanoparticles in ethanol are relatively more aggregated than in 1-propanol and that in methanol are more aggregated than ethanol, causing the surface of the resulting coatings to be rougher, which is why contact angles is increased with decreasing the carbon number and length of solvent. This morphological difference would be attributed to the difference in the aggregation states of the silica nanoparticles with the different type of alcohols.

The particle size distribution results agree well with this assumption and confirm the effect of alcohol solvent on surface morphology of silica nanoparticles (**Figure 21**). It can be seen that the silica nanoparticles tend to form larger aggregates in the less hydrophobic alcohols with the shorter hydrocarbon chains. The average sizes of the silica nanoparticle aggregates were approximately 629 nm in methanol, 486 nm in ethanol and 412 nm in 1-propanol. That is, the differences in dispersing ability would affect the level of aggregations of silica nanoparticles in solvent.

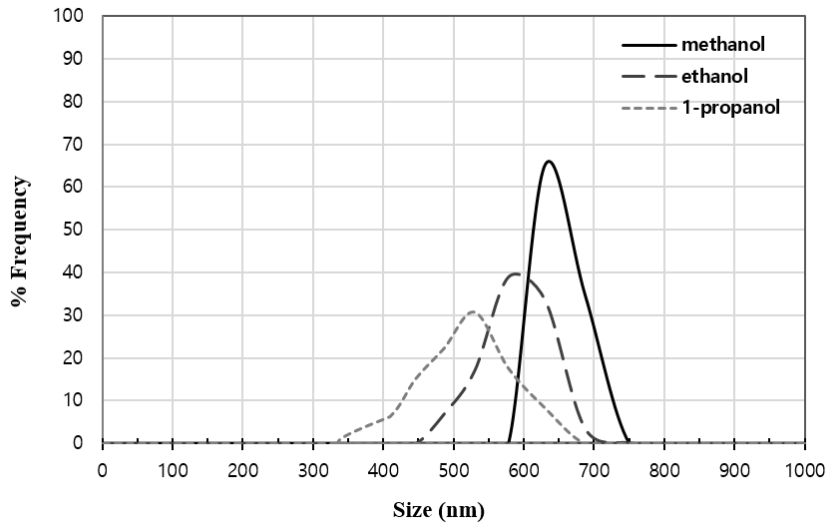

Figure 21. Particle size distribution of suspension containing the silica-nanoparticles using methanol, ethanol, and 1-propanol.

Table 4. The mean diameter and standard deviation of silica nanoarparticles in three different solvents; 1-propanol, ethanol, and methanol.

Solvent	Mean diameter (nm)	Standard deviation (nm)
1-propanol	412	232
ethanol	486	156
methanol	629	84

To confirm a dispersion ability of superhydrophobic treated silica nanoparticles in the different solvents, UV–vis absorbance at each cases were characterized at 600 nm and depicted in **Figure 22**. With the silica nanoparticles dispersed in the three different solvents, the dispersing power in the 1-propanol solvent was significantly higher than that in the other two solvents (ethanol and methanol). Optical density at 600 nm of the 1-propanol solvent containing silica nanoparticles was about 1.38, which is 3 and 9 times higher than that of ethanol and methanol, respectively.

The dispersing power of the solvent could also be affected considerably by their tail length because the hydrophobic tail groups enhances the attraction to the superhydrophobic treated silica nanoparticle surface. However, with decrease of the carbon chain of the alcohol solvents, the hydrophilic head group, –OH, which provided greater repulsive forces between the individual silica nanoparticles. Therefore, the hydrophobic silica nanoparticles aggregated more in lower alcohols and that led to the differences in surface roughness, which determined the degree of hydrophobicity of the coated surface of cotton fabric.

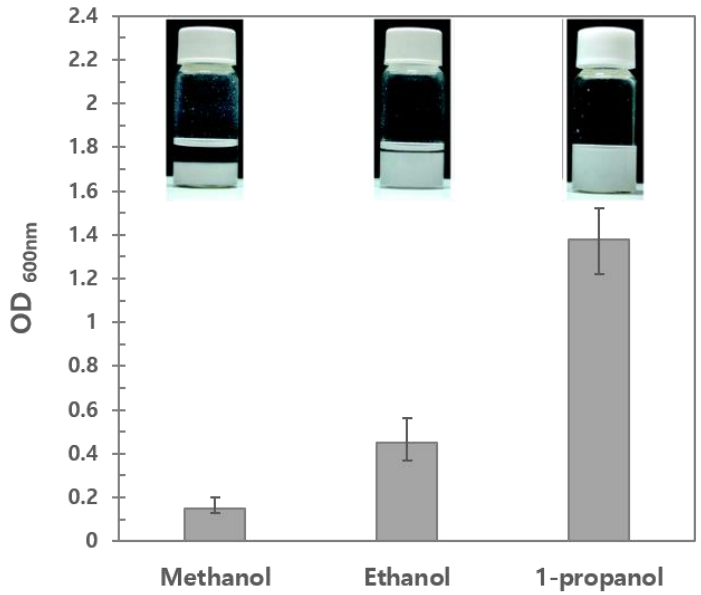

Figure 22. Dispersion ability of superhydrophobic treated silica nanoparticles in methanol, ethanol, and 1-propanol detected using UV-vis spectrophotometer at 600 nm.

Table 5. The optical density and deviation of silica nanoparticles in the alcohol solvents; 1-propanol, ethanol, and methanol from UV-vis spectrophotometer.

Solvents	Methanol	Ethanol	1-propanol
Optical Density at 600nm	0.15	0.45	1.38
Deviation	0.05	0.14	0.18

The washing durability of the superhydrophobic treated cotton textiles in the three different alcohols was analyzed using the water contact angles and sliding angles (**Figure 23**). The superhydrophobicity of the cotton fabrics after washing treatment were lost. The water contact angles of all the treated fabrics were reduced down below 150°, and the sliding angles show the quite high values. The coatings which realized in this study are not chemical interaction but physical bonded states. Therefore, the mechanical durability does not seem very strong. Also, the existence of the detergent somewhat deteriorated the hydrophobicity of the cotton fabrics.

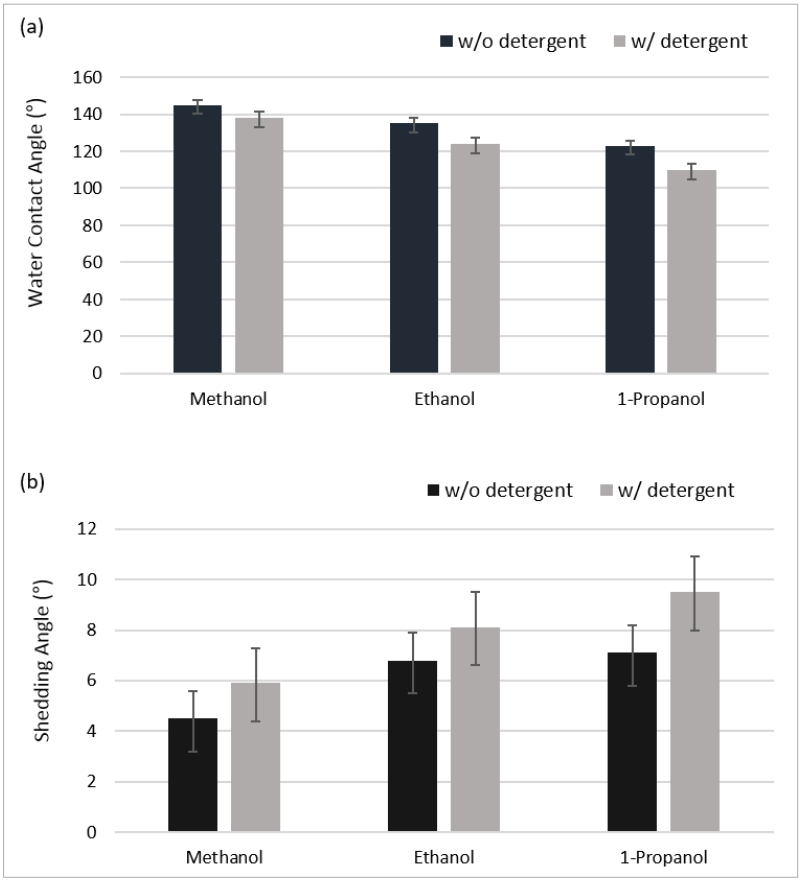

Figure 23. (a) Water contact angles and (b) sliding angles of the super-hydro phobic treated cotton fabric after washing treatment with and without detergent.

The water contact angle of the back side surface of the spray-coated cotton fabric in methanol was characterized and their water droplet were depicted in **Figure 24 (a)**. While the silica nanoparticles treated up-side surface showed the superhydrophobic behavior with contact angle higher than 170 degrees in **Figure 24 (c)**, the back side from that exhibited hydrophilic property with the water contact angle about 43°.

Recently, it has become customary to call a fabric with two faces a ‘‘Janus’’ fabric, named after Janus, who was depicted as having two opposite and distinct faces. Janus fabrics present a number of fascinating properties related to their asymmetric structures. Only recently has this type of fabric been of interest, and thus only a few literatures about Janus fabrics have been reported [120]; however, it is really a prospectively multifunctional entity especially due to their unique wetting characteristics.

This resultant Janus cotton fabric displayed antisymmetric wetting behavior: on one side, the pristine cotton fabric exhibited hydrophilic behavior, on the other side, the silica spray coating on the opposite side of the fabric was converted to a superhydrophobic surface. This simple strategy combined the production of hierarchical geometric architectures by nanoparticles spray-coating and the low surface energy of the silica nanoparticles treated with the hydrophobic material, which opens a new route for the design and development of functional smart fabrics from inexpensive and commercially available materials.

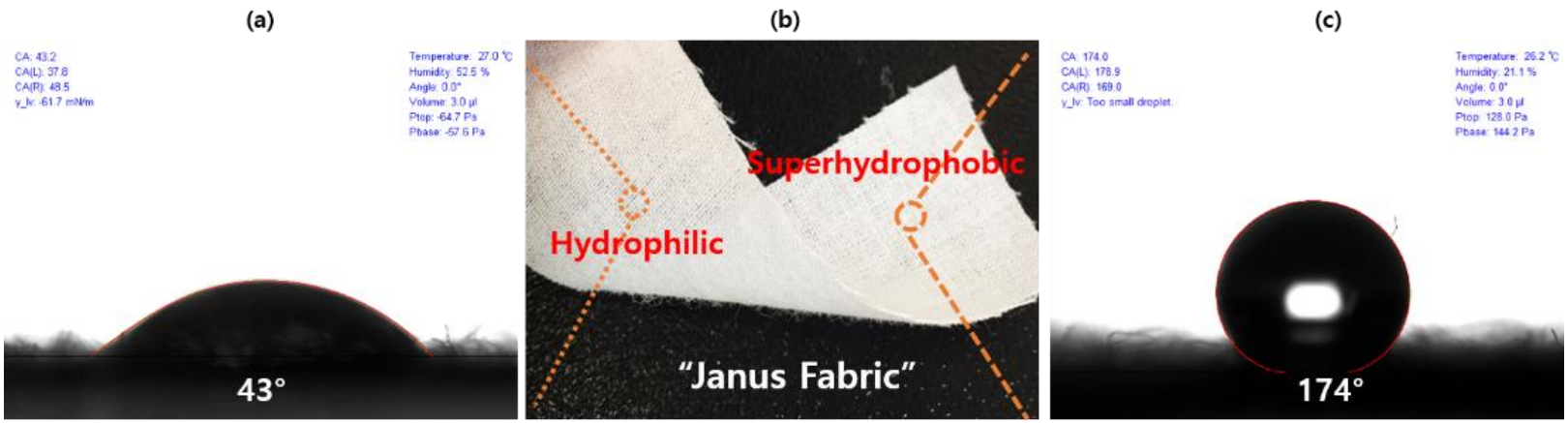

Figure 24. Biphasic Janus cotton fabric. (a and c) water droplet images and contact angles of the back side from spray-coated cotton textile (a) and (c) up side, respectively. (b) Photograph of the free-standing biphasic Janus fabric displaying antisymmetric wetting behavior.

Figure 25 (a) showed the photographs of a water droplet of 3 μL touching and leaving the cotton fabric coated with silica nanoparticles in methanol. The droplet was forced to sufficiently contact the cotton surface with an obvious deformation, and it was then lifted up. The corresponding photographs of the water droplet showed almost no deformation when leaving the aerogel surface, thus confirming the extremely low water adhesion for superhydrophobic cotton textile. Simultaneously, the pristine cotton fabric behaved as a hydrophilic property. As demonstrated in **Figure 25 (b)**, when a 3 μL water droplet contacted the pristine cotton surface, it stuck on the fabric and separated from the needle. The whole process was complete within 2 s, suggesting the well formed superhydrophobic surfaces on hydrophilic cottons by simple spray-coating.

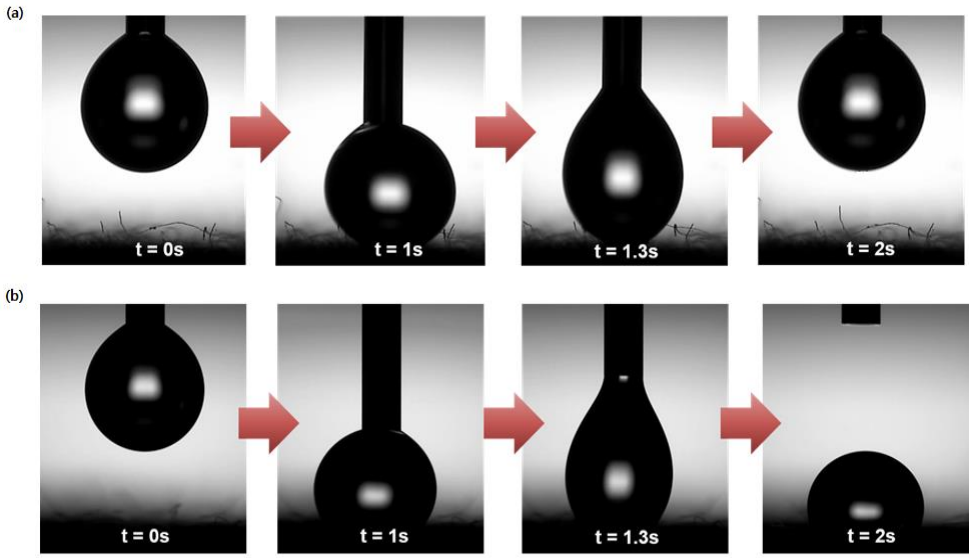

Figure 25. Photographs of dynamic measurements of water adhesion of (a) the cotton fabrics coated with silica nanoparticles in methanol and (b) the pristine cotton textile.

Considering the cotton fabrics as wearable textiles of fashion, the transparency of the superhydrophobic coating on the fabrics is very important. The transparency of the spray-coating on the cotton fabrics with methanol containing the hydrophobized silica nanoparticles can be identified in **Figure 26**. Compared to the pristine cotton textile, it can be concluded that the visibility after the coating processing was not varied. Also, with increasing volume of the water droplets, the coated cotton fabric did not get wet at all and retained a spherical shape (**Figure 27**).

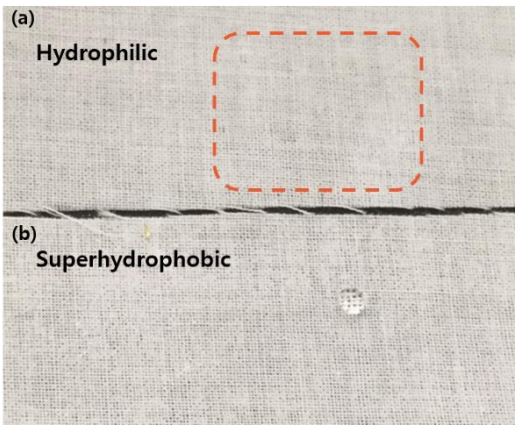

Figure 26. Photographs of (a) pristine cotton fabric and (b) coated cotton fabric by silica nanoparticles in methanol on which a water droplet maintained a spherical form. Red square area indicated a region of water absorbed.

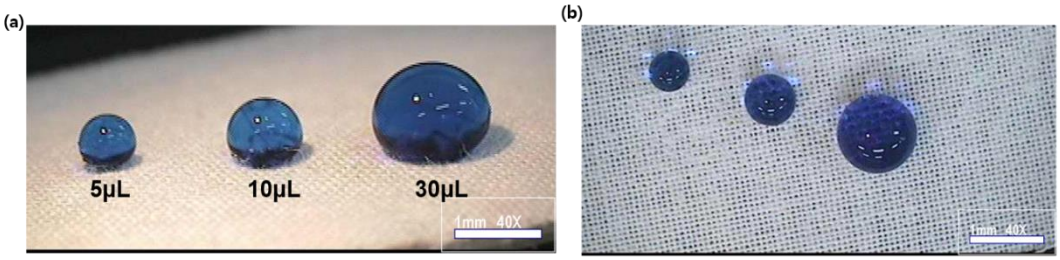

Figure 27. Photographs of water droplets with the three different volumes, 5 10, 30 μl from the left to the right on a cotton fabric coated by silica nanoparticles using methanol. (a) side view; (b) top-down view.

2.4 Summary

We have successfully obtained the extremely water-repellent surfaces on cotton fabrics by introducing the hierarchical morphology of both nanometer- and micrometer-sized roughness formed from hydrophobized silica nanoparticles. The coated cotton textiles in methanol exhibited the high contact angles, the low hysteresis, and good water repellency. The factors which determines the hydrophobicity of the coatings in the different alcohol solvent are the differences in surface roughness as well as surface energy of the fabric. To achieve superhydrophobicity, the presence of hierarchical surface topology has proven to be effective. The superhydrophobic and transparent coatings can be fabricated by the spray-coating method. This approach is applicable to a variety of surfaces including textile fabrics, paper, wood, etc. but needs to be overcome the durability issues.

Ⅲ. Superhydrophobic Electrospun PVDF Nanoweb

3.1 Introduction

Recently, the superhydrophobicity of textile materials has been intensively studied. The development of new fabrication techniques, which allow manipulating of surface morphology on the micro- and nano-levels, has significantly been increased. There are several technologies widely used in the textile industry to produce fibers with diameter in a submicron and nano ranges. Among them, electrospinning can generate fibers with diameter as low as 10 nm from any viscoelastic liquid that can solidify and allows functionalization of fibers with a wide range of additives [39]. In addition to flexibility in raw material selection, electrospinning is a cheap and simple method that has many options to control fiber diameter, morphology, surface topology, and fiber arrangements, and has been successfully scaled up for mass production. Since nonwoven webs composed of small fibers fabricated by electrospinning system are very similar to the superhydrophobic surfaces of plants leaves, it can be utilized to fabricate artificial self-cleaning surfaces [40].

So far, many types of relatively low surface energy materials including fluorinated materials, polystyrene (PS), poly(dimethylsiloxane) (PDMS), polyhedral oligomeric silsesquioxane (POSS), PHBV, and methyltriethoxysilane, have already been electrospun into fibers solely or blended with other materials to make a superhydrophobic surface. Fluorinated materials are of particular interest as

selfcleaning surfaces or stain-resistant textiles due to their extremely low surface energies.

In addition to the raw material selected, the final properties of electrospun fibers greatly depend on the processing parameters. Fibers with different diameters, morphology, secondary structures on a surface, and different fiber arrangements can be produced by varying electrospinning conditions [41]. Uniform nanofibers are preferred for most applications, although the formation of beads or microparticles is usually considered a defect. However, in the field of the superhydrophobic materials, beaded fibers and particles are often favored. Singh et al. [42] report the electrospinning of highly fluorinated poly[bis(2,2,2-trifluoroethoxy) phosphazene] to form nonwoven mats with high surface hydrophobicity. The contact angle increased with a decrease in fiber diameter and reached a superhydrophobic state as both beads and fibers were formed on the surface of the spun mats. The extremely high hydrophobicity of these surfaces is a combined result of surface enrichment with fluorinated units together with the inherent surface roughness associated with an electrospun mat.

Ma et al. [43] combined electrospinning and initiated chemical vapor deposition (iCVD) to produce superhydrophobic fabrics. iCVD is a one-step, solvent-free deposition technique that allows conformal coating of complex substrates. A poly(caprolactone) (PCL) mat comprising bead-on-string fibers, with ~100 nm average fiber size and ~2 μm bead size, was first electrospun and then coated by iCVD with a ~70 nm (nominally, as measured on a reference flat surface) conformal layer of polymerized perfluoroalkyl ethyl methacrylate (PPFEMA). The extremely

low surface energy of the PPFEMA coating (~9.3 mJ/m^2) and the high surface roughness inherent in the electrospun mats combined to provide stable superhydrophobicity with WCAs as high as 175° and hysteresis less than 2°.

Another well-known material with low surface energy is PS, which has been electrospun by several groups to make superhydrophobic surfaces. Jiang et al.[44] used solutions of polystyrene in dimethylformamide (DMF) with different concentrations keeping tip-to-collector distance and voltage constant and adjusting the feed rate. The solution with high viscosity (25% of PS by weight) allowed producing a web composed of smooth fibers with an average diameter of 420 nm, although the substrate produced from diluted solution (5% of PS by wt) was composed of microparticles (2–7 μm) covered with nanostructures (50–70 nm). The secondary structures created two-level surface roughness (microparticles/ nanostructures), so the static WCA on such film was 162° compared to 139° on the nanofiber web. However, the microparticle substrate had low mechanical integrity. Therefore, the authors used the 7% by weight solution of PS, which allowed the production of porous microparticles (3–7 μm) interlinked by nanofibers (60-140 nm). This substrate demonstrated a high static WCA of 160° and was more mechanically stable. The authors did not report dynamic behavior of water droplets on this surface.

Among the fluoropolymers, it has been known that the Teflon has the lowest surface free energy. Teflon and TeflonAF are nonelectrospinnable polymers because of their low dielectric constant values that prevents the generation of sufficient charge for the solution to be electrospun.Teflon does not dissolve in any solvents, and so

far no work has been reported on the electropinning of Teflon. Polyvinylidene fluoride (PVDF) is also one the most important fluorine-containing polymers. PVDF chemical structure is composed by the repetition unit $–CH_2-CF_2-$ along the polymer chain and it has better stiffness and mechanical strength than those of most fluorine-containing polymers. Moreover, it has exceptional chemical and thermal stability and high electric and chemical resistance excellent resistance to aging and durability, thus it has been widely applied in many regions including antifouling [45], air cleaning [46], rechargeable batteries [47] and sensors [48] etc.

For the past few years, a few studies have been reported on electrospun PVDF membranes for the superhydrophobic property. However, most of the reported PVDF based superhydrophobic surfaces are inorganic/organic hybrids, and not pure PVDF matrix. Superhydrophobic PVDF membrane with a contact angle larger than 150° was prepared by the electrospinning of the fluorinated silane functionalized PVDF [49]. Wang *et al* [50] fabricated a superhydrophobic surface with low water sliding angle (SA) and high water contact angle (CA) by electrospinning PVDF which was mixed with epoxy–siloxane modified SiO_2 nanoparticles. Superhydrophobic fluorinated POSS–PVDF-HFP nanocomposite coating on glass was perform by electrospinning by Ganesh *et al* [51]. Zhang et al. fabricated the superhydrophobic membranes for distillation via spraying a mixture of polydimethylsiloxane and hydrophobic SiO_2 nanoparticles on PVDF flat sheet membranes [52]. Although these methods have been developed to prepare superhydrophobic PVDF membrane, additional treatment such as phase separation [53], surface modification [54] and chemical vapor deposition [55], the complexity

and expensive cost of these methods may limit their practical applications.

This study focused on fabricating the hierarchical surface morphology from pure PVDF matrix by electrospinning without any surface modification or post-treatment. Superhydrophobic electrospun PVDF webs have been developed from the single step by electrospinning by controlling the surface roughness. Importantly, the ultrathin fibrous PVDF membranes were further applied for low cost, high efficient separation of oil and water emulsions, with the improved mechanical durability. This study contributes the development of advanced oil–water separation materials for practical applications and nanofiber web electrospun onto the conventional textiles for the manifestation of various functions without lamination process.

3.2 Experimental Section

3.2.1 Materials

PVDF pellets with the weight-average molecular weight of 180,000 g/mol and the number-average molecular weight of 71,000 g/mol were purchased from Sigma-Aldrich Co. (KOREA). N, N-dimethylformamide (DMF) (99.8 wt.% purity) and acetone were used as the solvents for the preparation of polymer solutions.

3.2.2 Preparation of Polymeric Solutions

The polymer solutions with a variety of concentrations of 8, 12, 16, and 20 w/v% based on the weight of PVDF were prepared to investigate of the effect of the viscosity on the surface morphology and the hydrophobicity of the electrospun fibrous films. The pre-weighted PVDF pellets were dissolved in a mixture of DMF and acetone with a volume ratio of 4:1. The blending solutions were obtained after sonication conducted for 3h and magnetic stirring subsequently for 12h at room temperature until a transparent homogeneous solution was obtained.

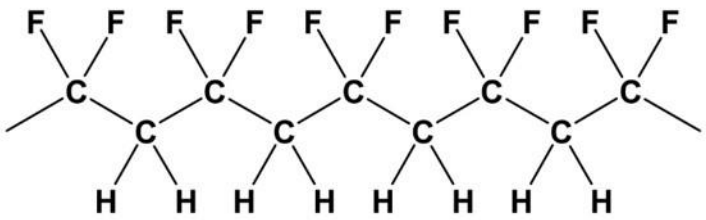

Figure 28. Chemical structure of polyvinylidene fluoride (PVDF).

3.2.3 Electrospinning

The prepared polymer solutions were electrospun into the fibrous morphology using the electrospinning system (Nano NC, KOREA). The homogeneous blending solutions were drawn into a plastic syringe (10mL) placed on the syringe pump (KDS200, KD Scientific Inc.).

The feeding rate of the polymer solution were controlled by the syringe pump at 0.1~0.5mL/h. The syringe was connected with a plastic nozzle having a diameter of 25 G (ID = 0.25 mm) through a PE tubing with inner diameter of 1.6mm. The electrospinning process was conducted at 13~15kV applied with a high voltage power supply (NANO NC, KOREA) across a distance of 10cm between the needle tip and the grounded electrode. The electrospun nanofibers were collected over a course of 3h in an aluminum foil to prepare the continuous fibrous membrane. All the experiments were carried out at room temperature and 30% RH. In order to eliminate any effect of residual solvents in the nanofibers web, the produced films were subsequently placed inside a fume cupboard under vacuum condition for overnight.

3.2.4 Solvent Casting

To investigate the effect of the surface structure by the electrospinning on the hydrophobicity of the PVDF membrane, the flat PVDF mats were prepared by the solvent casting method. The formulated PVDF polymer solution was transferred to a glass petri dish with a diameter of 60mm and the dish was placed in an oven heated at 323K for solvent evaporation. Then, the residual solvent was removed by keeping the formed membrane in a vacuum oven for 24h.

3.2.5 Hydrodynamic Test

The water repellency of the electrospun PVDF fibrous films and the PVDF membranes by the solvent casting were evaluated and compared by water contact angles, tilting angles, and hysteresis using a contact angle meter (SmartDrop, Femtofab). For the contact angles measurement, water droplets of the volumes of 1, 3, 5, and 10μL were dispensed using micropipette onto the manufactured membranes. The contact angles were obtained by measuring at five different positions of each four water volumes and the averaging values were obtained as water contact angle (WCA).

For the contact angle hysteresis analysis, the advancing and receding angles were obtained using the tilting plate method. The sliding angles were determined by placing a water droplet of 5.0μL on the surface of each membrane, which was then gradually tilted until the sessile drop began to slide. Just then, the hysteresis was measured by subtracting a receding angle value from an advancing value (θ_{adv} - θ_{rec}).

3.2.6 Characterization

The surface morphology of the electrospun PVDF fibrous films and the membranes by the solvent casting were analyzed using a field emission scanning electron microscopy (JSM-7600F, JEOL) at 2-3kV. Prior to the scanning electron microscopy observations, the membranes were vacuum dried for 2h. The sample were mounted on the sample studs by carbon double–sided adhesive tapes and sputtered with a platinum for 100 seconds by an automatic sputter coater (108 ATUO, CRESSINGTON). The compositions of the membranes were measured by an energy dispersive spectrometer (EDS, Quanta 200). The fiber diameter was analyzed from SEM images by Image J Software.

The topography of the PVDF membranes surfaces were characterized by atomic force microscope (XE-100, Park SYSTEMS). Air-dried membrane sample was fixed on a specimen holder and an area of 10 μm X 10 μm was scanned using the tapping mode. Surface roughness parameters as Ra, Rq, and Rz were calculated from the roughness profile determined by AFM. All measurements were performed in air at room temperature. The thickness of ten electrospun membranes was measured by using vernier calipers. The thickness of single layer film was measured by averaging the ten values at different positions of each membrane.

The rheological properties of each polymeric solution were performed using an AR 2000 Rheometer (TA Instruments, KOREA). For the very dilute solutions, the shear stress was characterized in the range of shear rate from 0.1 to 1000 s^{-1} in the cylindrical system using the cup and bob geometry at room temperature.

Fourier transform infrared spectroscopy (FTIR) spectra of PVDF samples were

obtained by a Fourier transform infrared spectrometer (FT/IR-410, JASCO, Japan). FTIR measurements were carried out by the KBr pellet method. The a- and b-phases of PVDF were associated with the vibration band peaks at 766 and 840 cm^{-1}, respectively. The fraction of the b-phase was determined by comparing the absorbance of vibration band peaks of the samples at 840 and 766 cm^{-1}.

The tensile characteristics of the fibers were evaluated using a universal tensile machine (UTM Instron-5543), load cell 1 kN. The strain rate was 2 mm/min, the initial length between the clamps was 30 mm. All samples were cut in the direction of collector rotation with dimensions of 10 mm × 30 mm and a thickness of ca. 100 μm. For the sake of statistical significance 10 specimens of each sample were tested, after which the average values of Young's modulus, the ultimate stress and maximum deformation at break were determined.

To examine the water–oil separation capability of the fibrous PVDF membranes, a separation setup consisting of a Buchner funnel and a suction flask was built. The fibrous PVDF membrane with a permeation area of 8.04cm^2 was used as the membrane and the surfactant-free oil-in-water emulsion was prepared by mixing 30 ml of water and 30 ml of benzene. The mixture was emulsified by a high-speed homogenizer for 30 min at 400 rpm and was further homogenized by an ultrasonic treatment for 20 min to form a milky emulsion. The prepared oil-in-water emulsion was poured onto the fibrous PVDF membrane without external driving force. To examine the emulsified droplets in oil-in-water emulsion, a video microscope system (STVM-0001 with magnification of 300) was employed before and after the filtration process. The droplet sizes of the oil-in-water emulsion before and after

the separation procedure were measured by Particle size analyzer (Nanotrac, MicrotracTM). The averages of 3 different measurements of each were recorded and averaged.

The oil absorption capacity values, W, were obtained by measuring the mass of the electrospun dry PVDF membrane and then measuring the mass of the absorbed oil. The ratio of the absorbed oil mass to the initial superhydrophobic PVDF membrane mass was taken as the W value, averaging out three samples. To ensure full saturation was obtained before weighing, the samples were left submerged in the oil (without water) overnight. The samples were then removed with sharp needle tweezers and immediately placed onto a weigh paper to be measured on the mass balance. Then the oils absorbed in the superhydrophobic PVDF membranes were removed by immersion in acetone, and the membrane was used to repeat the above cycles. The oil-absorption capability of the electrospun PVDF membrane were measured at every 3, 5, and 10 oil absorption cycles. After each oil absorption cycle, the membrane was retrieved by washing with acetone or other organic solvents followed by drying in an oven.

3.3 Results and Discussion

The electrospinning process was performed from the polymeric solutions with the varying PVDF concentrations. The **Figure 29** show the effect of polymer concentration on the surface morphologies and the fiber diameter. In the case of the low polymer concentration (8 wt%) of the PVDF solutions, it can be seen that the surface of the electrospun web consists of the nano-sized particles and ultrafine fibers. The average diameter of the fiber is very thin 30 nanometers and the fiber formation is very weak and unstable. It shows that the density of PVDF is too low to form the stable fiber diameter.

As the concentration of the PVDF polymer solution increases, it can be clearly observed that the shape of the bead particles became clear and larger and the fiber had a thicker with uniform diameter. The bead-on-string structures, i.e., beaded fibers can be seen. For the electrospun PVDF web with 12 wt% concentration, the elliptical bead structures are shown in the nano-size range and it gradually increased to micro-size at 16 wt%. The fiber diameter became thicker with increased concentrations of electrospinning solutions, the beads on the fibers eventually disappeared and the surface structure consists of the well-defined nanofibers at a high polymer concentration of 20wt%.

The fiber diameter distributions diagram and the average size of the surface morphology at different concentrations of electrospinning solutions in **Figure 30** have also confirmed these morphology changes. Particularly, it can be seen that the hierarchical structure composed of microbeads and nano-scaled fibers was formed

at a concentration of 16 wt%.

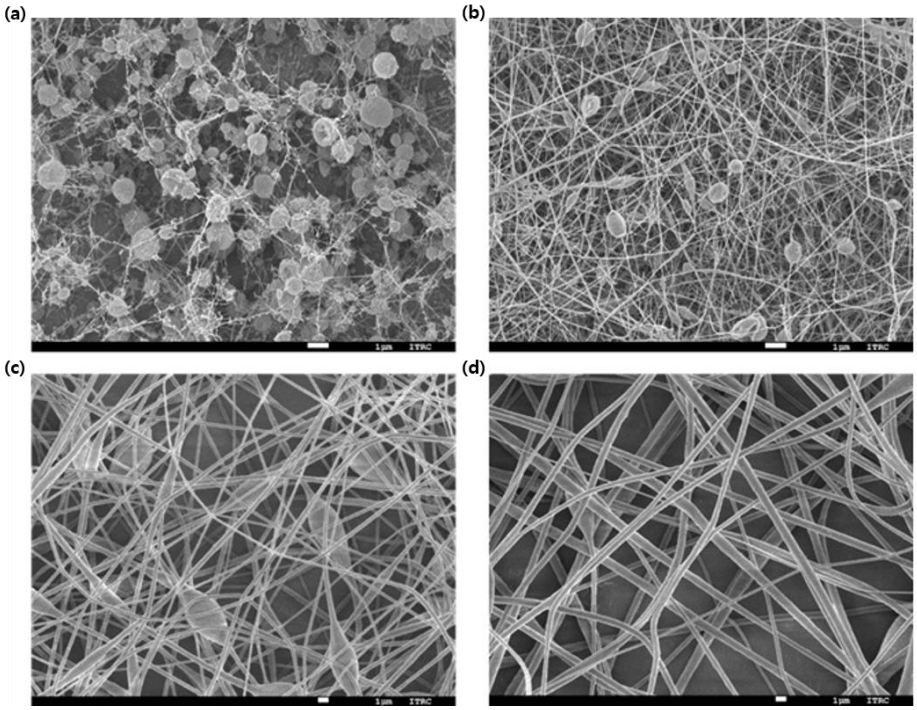

Figure 29. FE-SEM images of PVDF fibrous films by electrospinning of (a) 8 wt%, (b) 12 wt%, (c) 16wt%, and 20 wt% concentrations. SEM micrograph magnification is 3,000 x.

(a) 8 wt%

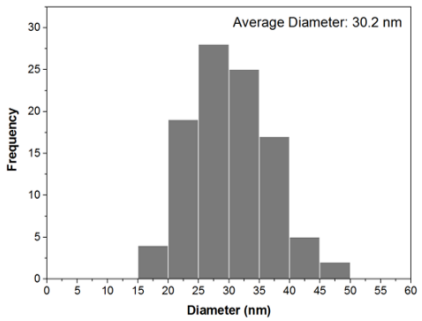

	Fiber diameter(nm)	Beads size(nm)
Mean	30.254	453.65
SD	6.62	329.129
Min	15.673	137.497
Max	48.11	795.392

(b) 12 wt%

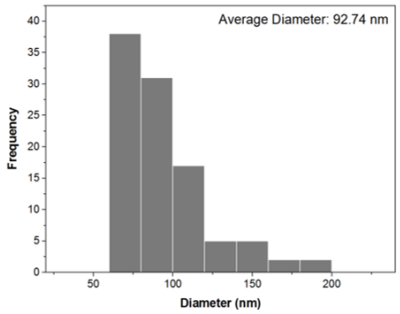

	Fiber diameter(nm)	Beads size(nm)
Mean	92.74	605.51
SD	27.397	198.74
Min	60.218	464.38
Max	188.03	866.144

(c) 16 wt%

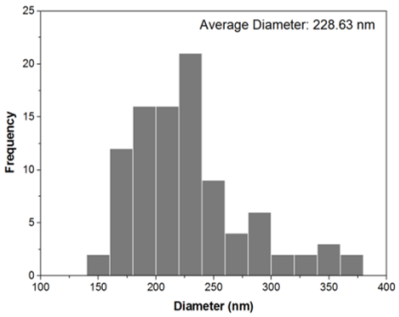

	Fiber diameter(nm)	Beads size(μm)
Mean	228.636	10.785
SD	49.764	1.976
Min	153.251	8.068
Max	379.602	12.488

(d) 20 wt%

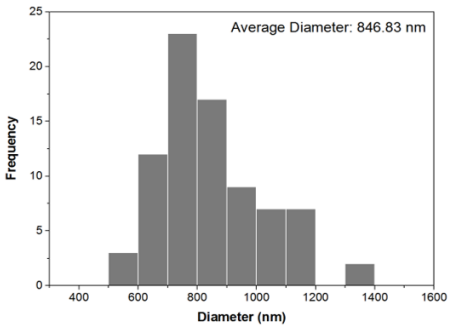

	Fiber diameter(nm)	Beads size
Mean	846.833	-
SD	175.661	-
Min	545.261	-
Max	1340.638	-

Figure 30. The fiber diameter distributions diagram and the average size of the surface morphology of (a) 8 wt%, (b) 12 wt%, (c) 16 wt%, and (d) 20 wt% concentrations of electrospinning solutions.

It has been shown in the literature that the concentration of the electrospinning solution has a significant effect on the fiber morphology and the diameter of the synthesized nanofibers [56]. In order to confirm the effect of viscosity on the surface morphology of the PVDF fibrous web, the rheological properties of PVDF solutions at different concentrations were characterized in **Figure 31.**

First, variations of the shear stress over the shear rate in a range from 0.1 to 1000 s^{-1} of the polymeric solutions were measured. All the PVDF solutions with the different concentrations showed the non-Newtonian fluid behaviors and exhibited shear thinning phenomena. The simple linear relation between shear stress and shear rate of the polymeric solutions can be shown at the low shear rate region lower than 100 s^{-1}. In the above region, we can see a non-linear increase in stress with increasing rates of shear, where the slope is given by the viscosity of the fluid. The plots of viscosity versus shear rate were obtained in **Figure 31 (b)**. The viscosities remained constant in the low shear rate range and it decreased as the shear rate increases, showed shear thinning behaviors. These non-Newtonian phenomenon certifies the existence of chain entanglement forces between molecules, which is useful for the electrospinning process.

The viscosity of the PVDF polymer solution increased with increasing polymer concentrations. In **Figure 31 (b)**, the viscosity of 20wt% PVDF solution was low about 1.5 Pa S and 50 times greater than that of 8wt% solution as 0.03 Pa S.

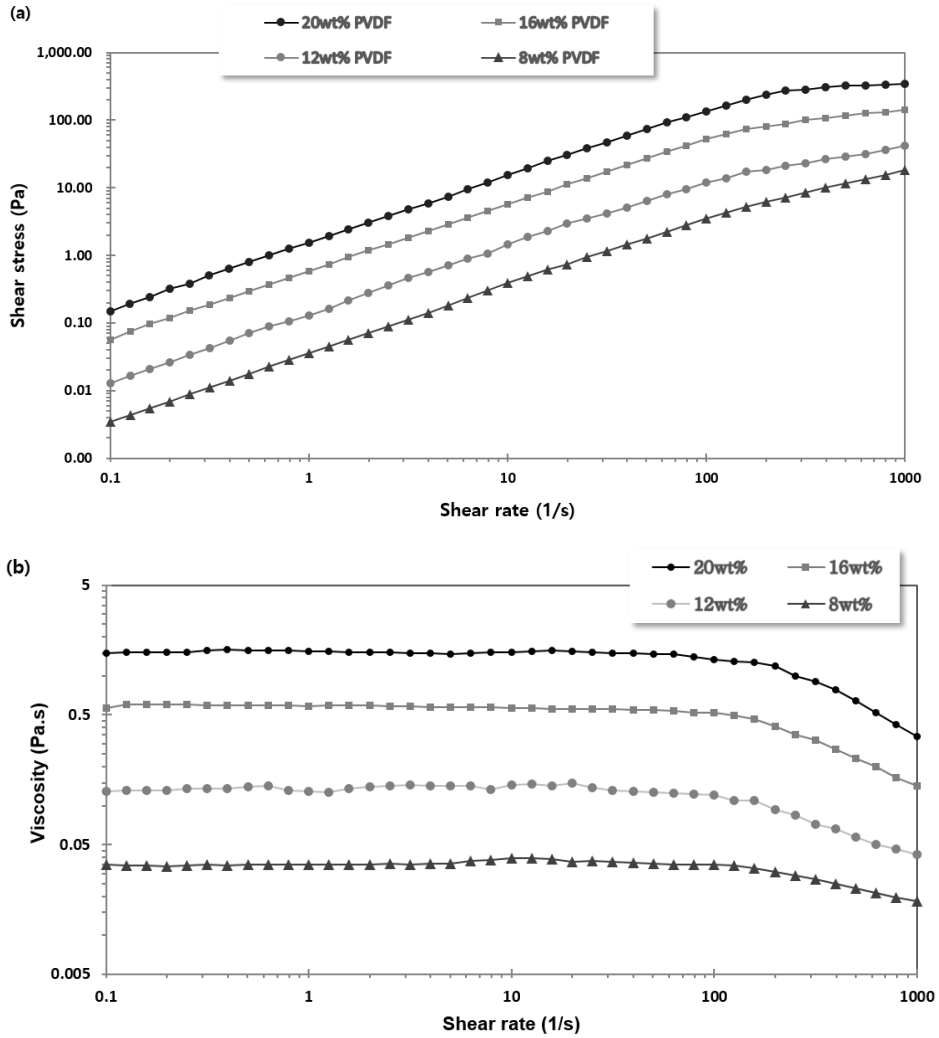

Figure 31. Steady flow curves of (a) shear stress and (b) shear viscosity with respect to the varying shear rate for the PVDF solutions from the different PVDF concentrations.

As shown in the literature [57], the higher viscosity of the increased polymeric concentrations would favor the formation of thicker fibers due to the stronger intermolecular interactions in the homogeneous solutions. The value of viscosity characterizes chain entanglement forces between molecules. Thus, the change in viscosity means that there is an increased chain entanglement within the PVDF polymeric solutions.

As the concentration of the PVDF solution increased, the viscosity of the electrospinning solution increased thereby increasing the average diameter of the electrospun fibers and the size of bead particles as well. Viscosity is known to play an important role in electrospinning process and hence controlling the diameter and structure of the spun fibers. Moreover, it can be confirmed that formation of the fiber and bead structure of the electrospun surfaces can be effectively controlled by the polymer concentration, or the viscosity of the spinning solutions. As mentioned earlier, the hierarchical structure with micro- and nano-scaled roughness is very effective to increase the hydrophobicity. It can be seen that he PVDF web with the hierarchical roughness were adequately produced from the 16wt% PVDF solutions using electrospinning process.

To investigate the effect of the surface roughness on the hydrophobicity of the electrospun PVDF webs, the PVDF membranes with different concentrations were observed by AFM at tapping mode as shown in **Figure 32**. The surface structures found with the AFM measurement correlate well with the FE-SEM images. In lower concentrations of 8 and 12 wt%, a well-defined structure composed of beads or fibers was not observed and height profiles show the relatively flat surface.

Meanwhile, the surface topology of the electrospun PVDF membrane with 16 wt% concentration, the bumps caused by nanofibers and micro-sized bead structures have higher heights, and larger distances exist between each bump, which may make the surface more hierarchical structured, i.e., more hydrophobic. The existence of the bumps on the PVDF surface led the higher probability of air pockets formation and thus enhancing membrane hydrophobicity. Additionally, the bumps structure features disappeared when the thick fiber were electrospun at 20 wt% concentrations and the smooth surface can be shown in height profile in **Figure 32 (d)**. As a result, the surface roughness and topology of electrospun PVDF membranes can be varied and controlled by changing the concentrations.

The surface roughness parameters shown in **Table 6** indicated the similar tendency with the SEM results. In case of electrospun membrane comprising of nanofibers at 20 wt% concentration, it can be seen that surface roughness has the lowest value as 0.292 μm. Also, the PVDF webs composed of nanoparticles at 8 wt% concentrations had the low surface roughness parameter of 0.321 μm. The surface roughness has been increased as the bead-on-fiber structures were formed. That is, the roughness parameters at 12 wt% concentration was 0.693 μm and it gradually increased to 1.224 μm at 16 wt% concentration.

From the AFM results, it can be confirmed that a combination of highly hierarchical micro- and nanostructures were successfully formed on the fiber surface from the electrospinning solutions with adequate compositions. That is, the hierarchical morphology aroused from nano-scaled fibers and micro-sized beads are increased, which may provide more air pockets and make the surface superhydrophobic.

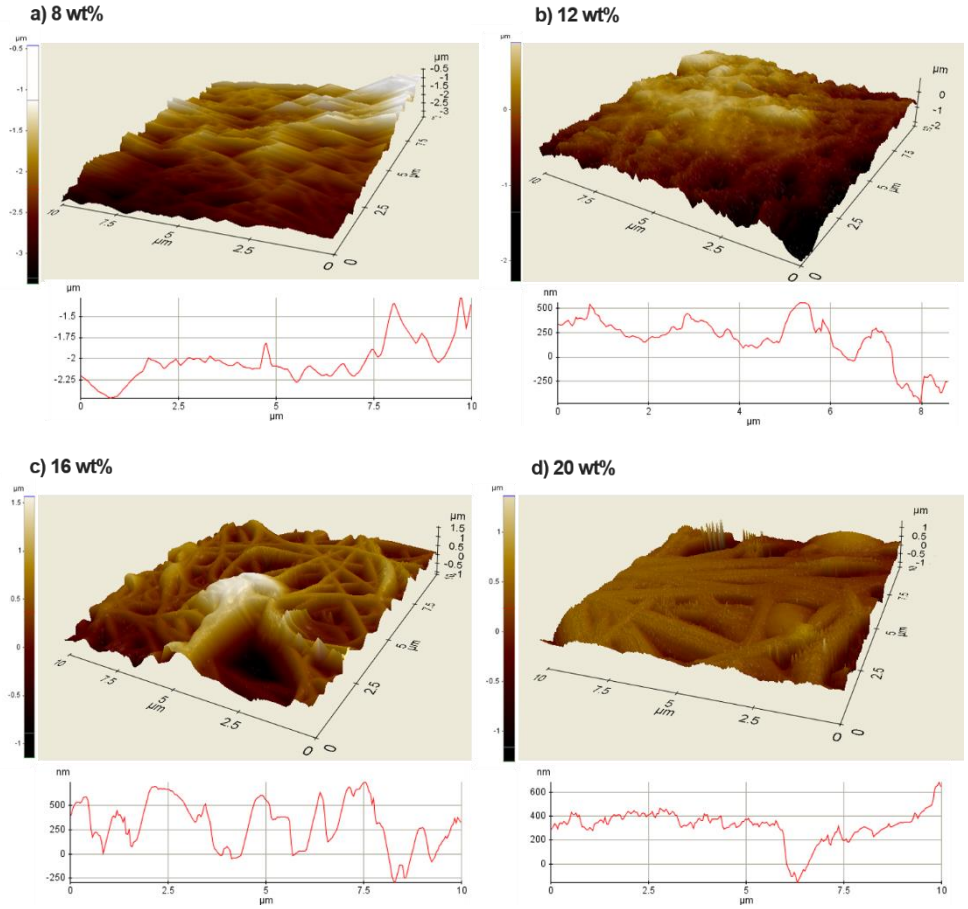

Figure 32. AFM 3D images and cross-sectional profiles in a given location of electrospun PVDF membrane surface with different concentrations (a) 8 wt%, (b) 12 wt%, (c) 16 wt%, and (d) 20 wt%.

Table 6. Roughness parameters obtained from AFM measurement for each PVDF membranes

PVDF films	Rq(μm)	Ra(μm)	Rz(μm)
8 wt%	0.416	0.321	2.78
12 wt%	0.832	0.693	4.321
16 wt%	1.425	1.224	6.282
20 wt%	0.395	0.292	2.688

R_q: Root mean square roughness
R_a: The mean roughness
R_z: Mean roughness depth

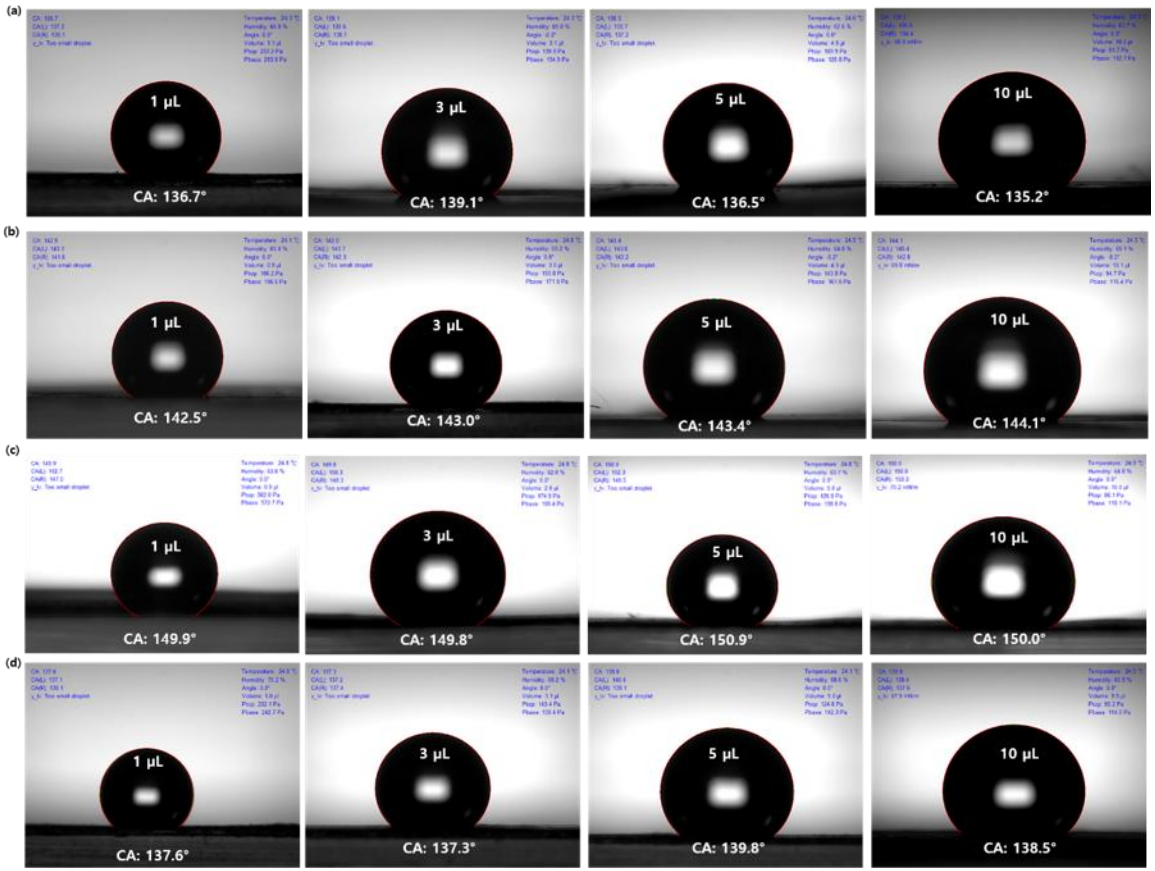

Figure 33. Captured images of the water droplets at varying volumes 1, 3, 5, 10µL placed on the electrospun PVDF fibrous web from the (a) 8wt%, (b) 12 wt%, (c) 16wt%, and (d) 20 wt% concentration solution.

The contact angle images of the electrospun PVDF fibrous web from the different concentration solution are presented in **Figure 33**. It has often been reported that the contact angle values changed significantly with the volume of the water. In order to compensate the water contact angle to the webs measured with the water volume change, the water droplets with the different volume of 1, 3, 5, and 10μL were deposited and water contact angles were characterized. However, with the change of the water volume, the measured values of the contact angles seem to remain constant**.**

In **Figure 32**, the water contact angles of the electrospun PVDF webs were schematically depicted. In the films consisting of only the nanoparticles (8wt%) or nanofibers (20wt%), the average water contact angle of the electrospun PVDF films had similar values around 137°. It is well known that beaded fibers or the bead-on-string structure tend to exhibit the increased hydrophobic property. It gradually increased to about 143° at 12wt% concentration of electrospun PVDF webs consisting of the nano-sized beaded fibers, and had the maximum values over 150° at the 16wt% concentration, i.e., in the hierarchical structures of micro-sized beads and nano-scaled fibers. As mentioned earlier, the hierarchical structure with micro- and nano-scaled roughness has increased the hydrophobicity of the electrospun PVDF webs.

Basically, all the contact angle values of the electrospun PVDF webs were over 135°, which verify the inherent hydrophobic property of the PVDF materials. The fluoro-polymers usually exhibit low surface energy, which may be attributed to intensive electronegative characteristics of the fluorine element. Thus, its attractive

force to other substances is weak. Due to its fluorinated composition, all the electrospun PVDF webs prepared in the work had the low surface energy and exhibit the high water contact angle values.

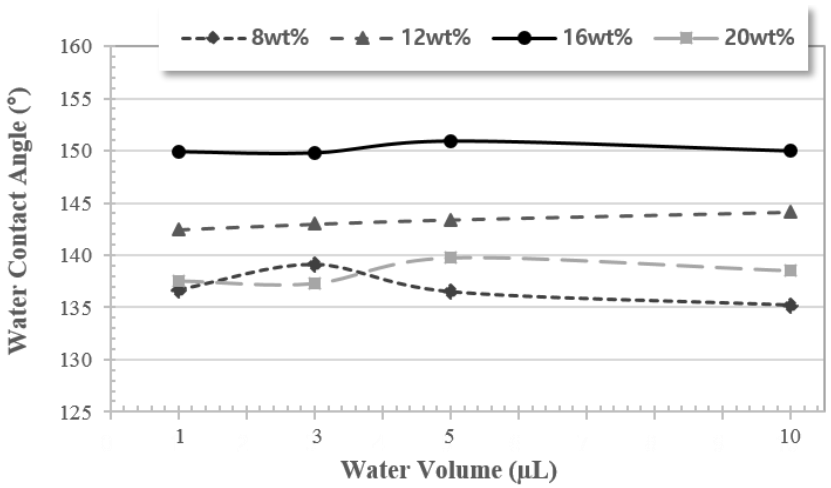

Figure 34. Water contact angles of the electrospun PVDF fibrous films of varying concentrations from 8wt% to 20wt% at the different water droplet volumes from 1µL to 10µL.

As mentioned earlier, the main factors that determine the hydrophobicity of the surface are surface energy and surface morphology. As the surface energy of the electrospun PVDF webs would be the same, the surface roughness from the different concentrations would have affected the hydrophobicity of the webs. In **Figure 35**, the correlation between the roughness parameters and the water contact angle can be seen. Depending on the concentrations, the surface roughness varied and the water contact angle also changed. Especially, they exhibit the same tendency with the change of the concentrations. The increased surface roughness affected by rheological properties at different concentrations of the fibrous PVDF membranes enhances the hydrophobicity.

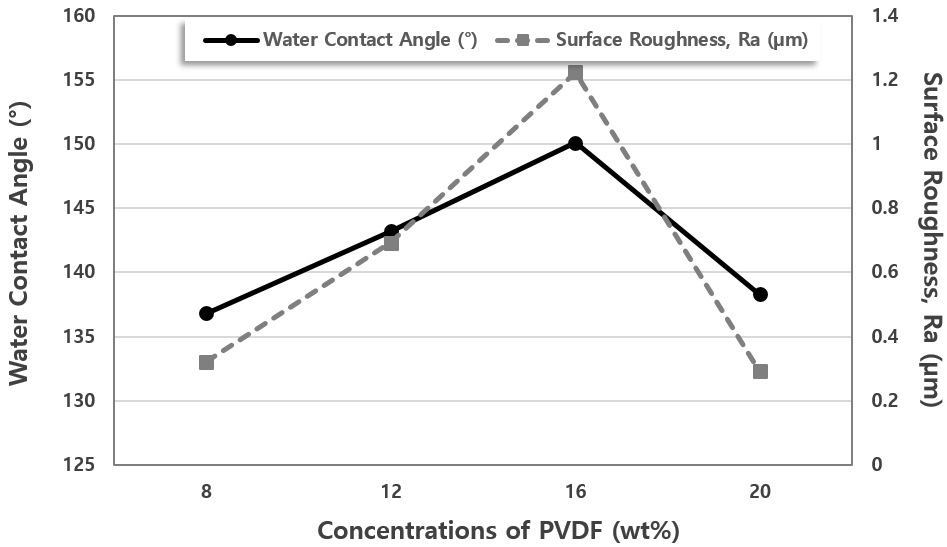

Figure 35. Effect of the surface roughness and concentrations of PVDF on the static water contact angle.

For the measurement of the tilting angle and hysteresis, the advancing and receding angles were measured until the water droplet on the electrospun PVDF films started to slide (**Figure 36**). The tilting angle was 20° at the electrospun PVDF films with 8wt% concentration, 18° at 20wt%, 14° at 12wt%, and 10° at 12 wt%. Because the lower tilting angle value means the more hydrophobic property, the hydrophobic tendency is agreement well with the water contact angle values. As the tilting angles increased, the differences between the advancing and receding angles became larger.

The contact angle hysteresis is defined as the difference between the advancing and the receding contact angles at a tilting angle on a solid surface. The wettability, water contact angle and hysteresis of the electrospun PVDF webs with the different concentrations are summarized in **Table 7**. It can be seen that the electrospun PVDF films of 16wt% concentration had the highest surface roughness and the most hydrophobicity, and followed by 12wt%, 20wt%, and 8wt% concentrations. Contact angle hysteresis can be arising from molecular interactions between the solid surface and the liquid droplet or from surface anomalies, such as roughness or heterogeneities [58]. Thus, the hysteresis has been affected by the surface roughness as well and the hierarchical morphology is essential to achieve the hydrophobicity.

Figure 36. Advancing and receding angles respect to tilting angle of the electrospun PVDF films from (a) 8wt%, (b) 12wt%, (c) 16wt%, and (d) 20wt% solutions. (below)

(a)

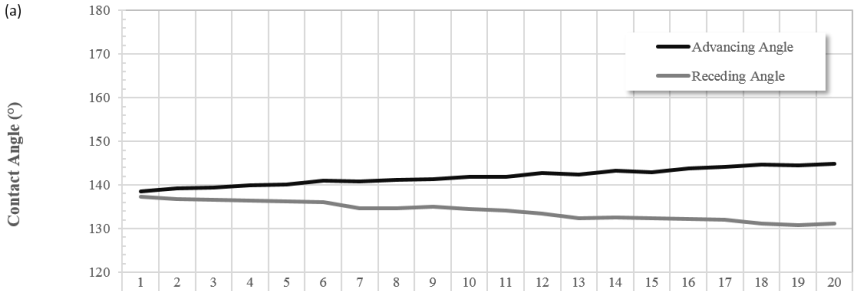

	1	2	3	4	5	6	7	8	9	10	11	12	13	14	15	16	17	18	19	20
Advancing Angle	138.6	139.2	139.3	140	140.1	140.9	140.9	141.1	141.3	141.9	141.9	142.7	142.4	143.2	143	143.8	144.1	144.7	144.5	144.8
Receding Angle	137.3	136.7	136.7	136.5	136.2	136	134.7	134.6	135	134.5	134.1	133.5	132.4	132.5	132.5	132.3	132	131.2	130.9	131.1

Tilt Angle (°)

(b)

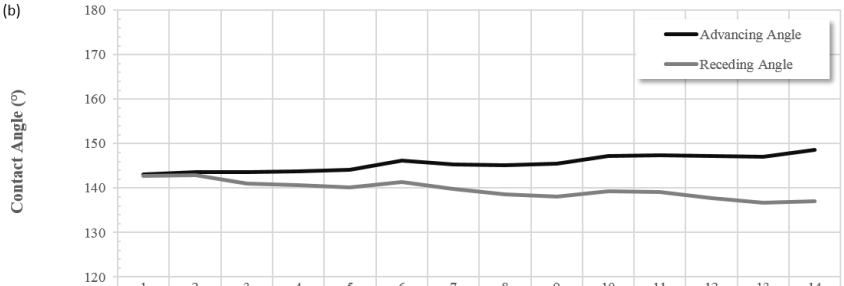

	1	2	3	4	5	6	7	8	9	10	11	12	13	14
Advancing Angle	143.02	143.67	143.65	143.77	144.18	146.09	145.34	145.17	145.49	147.23	147.46	147.21	147.01	148.64
Receding Angle	142.65	142.98	141.08	140.73	140.1	141.38	139.81	138.67	138.09	139.32	139.19	137.67	136.76	136.99

Tilt Angle (°)

(c)

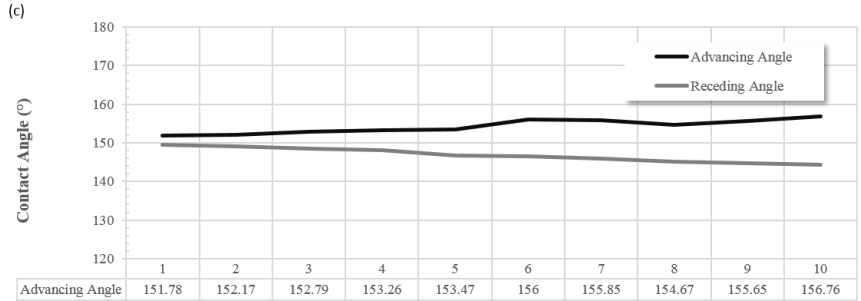

	1	2	3	4	5	6	7	8	9	10
Advancing Angle	151.78	152.17	152.79	153.26	153.47	156	155.85	154.67	155.65	156.76
Receding Angle	149.47	149.18	148.43	148.01	146.72	146.48	146	145.05	144.75	144.38

Tilt Angle (°)

(d)

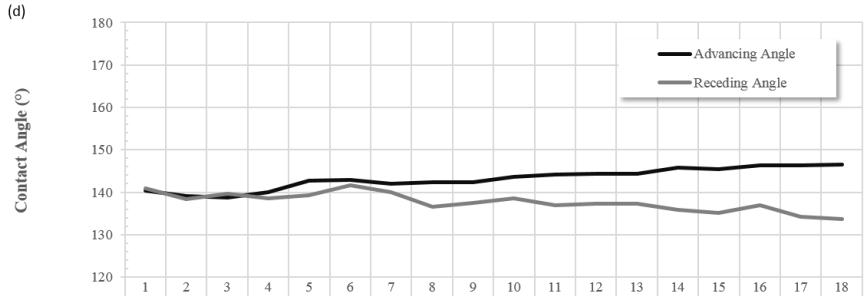

	1	2	3	4	5	6	7	8	9	10	11	12	13	14	15	16	17	18
Advancing Angle	140.3	139.1	138.8	140	142.8	142.9	142	142.4	142.3	143.7	144.2	144.4	144.3	145.8	145.4	146.4	146.3	146.4
Receding Angle	140.9	138.4	139.6	138.5	139.3	141.6	139.9	136.5	137.4	138.6	136.9	137.3	137.3	135.8	135.1	136.9	134.2	133.8

Tilt Angle (°)

Table 7. Surface roughness, water contact angles, sliding angle and hysteresis of the electrospun PVDF films with the different concentrations.

	8 wt%	12 wt%	16 wt%	20 wt%
Surface Roughness (μm)	0.321	0.693	1.224	0.292
Water Contact Angle (°)	136.87	143.24	150.16	138.30
Sliding Angle (°)	20	14	10	18
Hysteresis (°)	13.7	11.7	11.1	12.7

In order to identify the effect of the surface morphology on the hydrophobicity, the electrospun PVDF films with 16wt% concentration was prepared by a solvent-casting technique. The low surface roughness composed of the flat beads structure on the order of micrometers or less was revealed in **Figure 37 (a)**. As reported that the PVDF flat membrane with a contact angle of around 90° [59], the water contact angle of the PVDF film by the solvent casting was about 98°, indicating that the inherent PVDF exhibits hydrophobic property. However, compared with the electrospun PVDF web in **Figure 37 (b)**, the morphological difference was distinct. Although the both surfaces were made of the same material's composition, their surface structures showed the quite different roughness. Also, the water contact angle value of the electrospun web was about 50 degrees higher than that of the solvent casted film.

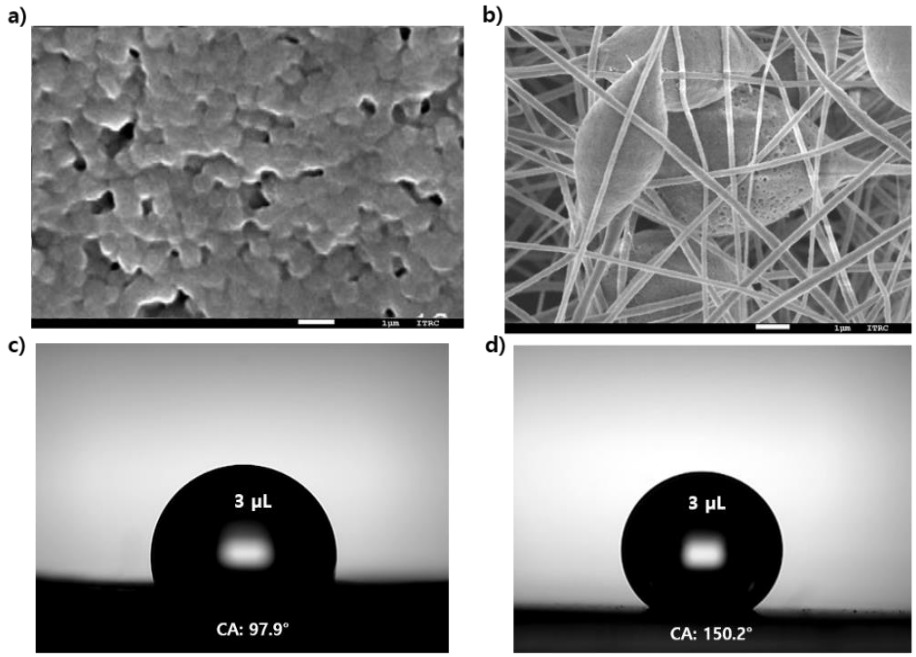

Figure 37. FE-SEM image of the PVDF flat film with 16wt% concentrations by solvent casting method (a) and the electrospinning process (b). The captured images of the water droplets of 3μL placed on the solvent casted film (c) and the electrospun web (d).

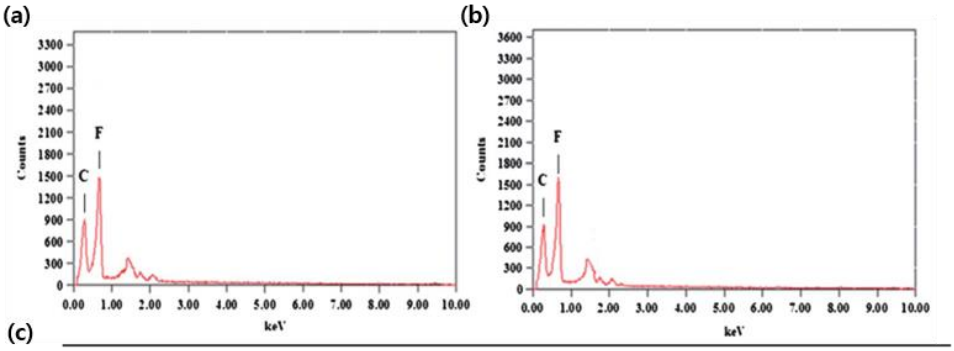

(c)

	Elemental composition (%)			
Surface	C	O	F	F/C
Electrospun films	57.88	0.35	41.77	0.72
Solvent casted films	54.4	0.29	45.31	0.83

Figure 38. EDS spectrum of (a) the electrospun PVDF web, (b) the solvent casted PVDF film, and (c) surface chemical composition of each.

Figure 38 show the energy dispersive X-ray spectra (EDS) of the electrospun PVDF web and solvent casted PVDF web of 16 wt%, and their XPS analysis. The energy dispersive spectrometer (EDS) results demonstrated that the surface chemical compositions were not affected by the fabrication process. That is, only the surface morphology appeared in the membranes had affected on the hydrophobicity of the webs produced in each methods and the hierarchical topology made from the electrospinning made the surface more water-repellent. The presence of a quite small oxygen amount (0.35% or 0.29%) may arise from the exposure of the PVDF films to the air or due to solvent contaminants.

PVDF is a semi-crystalline polymer with an amorphous phase and a crystalline phase and has two main phases at least depending on the preparation conditions, according to the chain conformations, trans (T) or gauche (G) linkages: α-type crystalline (TG+ TG-, monoclinic) and β-type crystalline (TTTT, orthorhombic), being the β phase the one with the largest piezoelectric response [60]. The crystalline structure of PVDF influences the polarity of PVDF. α Phase crystalline structure exhibits nonpolar behavior and β crystalline structure has polar properties. To obtain the piezoelectric β-phase, PVDF needs to be mechanically stretched to orient the molecular chains and then poles (placed under a strong electric field to induce a net dipole moment) under tension, which can be obtained during the electrospinning [61]. Thus, electrospinning is a simple technique to form the piezoelectric β-phase of PVDF directly from solution.

Figure 39 shows FTIR spectra of the solvent-casted PVDF film and electrospun PVDF webs. The crystalline peaks of PVDF-α and β phases have been determined

by FTIR vibration band. Vibration band peaks at 614 and 765 cm^{-1} were associated with α-phase crystalline structure of PVDF. The strong peaks at 840 and 510 cm^{-1} are the characteristic bands of b-phase crystallites of PVDF [62]. Compared with the solvent-casted PVDF film, the vibration band peaks of α crystalline phase at 765 and 614 cm^{-1} decreased while the peaks of β crystalline phase increased in electrospun PVDF webs. Meanwhile, the vibration band peaks at 840 and 510 cm^{-1} increased in electrospun PVDF sample but, its peaks decreased in solvent-casted film. The electrospinning method favors the formation of PVDF fibers crystallized in the electroactive β-phase, due to the higher electric fields during processing contribute to dipole alignment and consequently to electrical poling of the PVDF fibers, leading to high responsive piezoelectric fibers. It can be confirmed that the electrospinning process also increased the fraction of β-phase crystallites of PVDF.

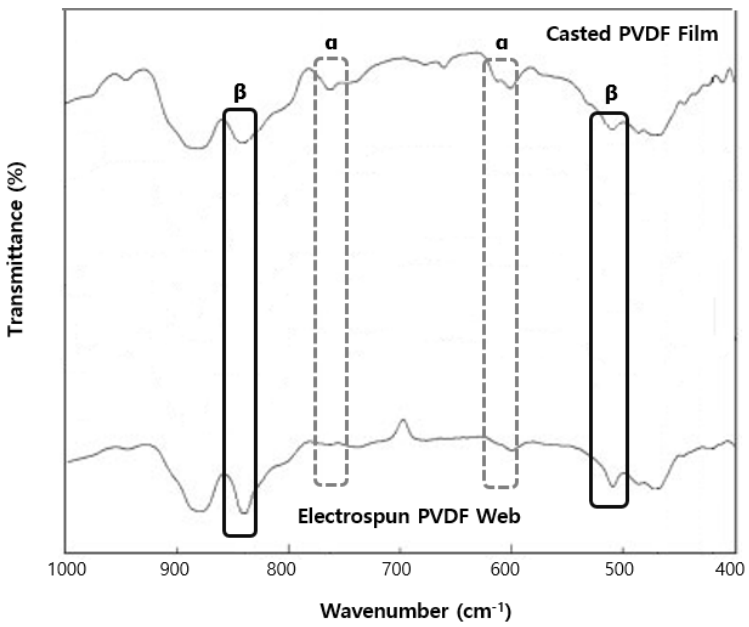

Figure 39. FT-IR spectra of the solvent-casted PVDF film and electrospun PVDF web.

The quantification of the β-phase content of the electrospun samples can be performed from the FTIR spectra applying and following the procedure explained in equation 6:

$$F(\beta) = \frac{A_\beta}{\left(\frac{K_\beta}{K_\alpha}\right)A_\alpha + A_\beta} \quad (9)$$

where F(β) represents the β-phase content, K_α and K_β the absorption coefficient for each phase and A_α and A_β the absorbance at 766 and 840 cm^{-1}, respectively. The absorption coefficient value is 6.1 × 10^4 cm^2mol^{-1} and 7.7 × 10^4 cm^2mol^{-1} for K_α and K_β, respectively [63].

(a)

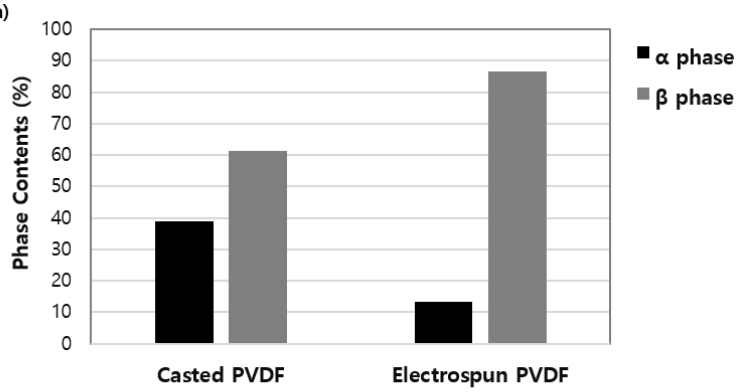

(b)

Sample	β/α
Solvent-casted PVDF	1.58
Electrospun PVDF	6.46

Figure 40. α and β phase content in the solvent-casted PVDF film and electrospun PVDF web (a) and ratio of the β-phase to α-phase of PVDF membranes.

Figure 40 shows the α- and β-phase contents and ratio of the β-phase to α-phase, which is calculated from the absorbance of the respective vibration band peaks of FTIR spectra (β-phase: 840 and α-phase: 766 cm^{-1}). The results indicate that only a small amount of α-type PVDF crystal exist in electrospun nanofibers, i.e., β-type crystallite dominates in electrospun nanofibers. In conclusion, electrospinning process increases the β-phase fraction of the PVDF membrane and the ratio of β/α. It is to notice that this increase of the β -phase content does represent a significant growth of the electroactive performance of the material. Gomes et al. [64] reported that the piezoelectric coefficient is proportional to the amount of oriented dipoles, and therefore the number of β-phase present in PVDF films influence the piezoelectric response of the material.

The mechanical properties of the fibrous membranes obtained by electrospinning depend on the diameters and morphology of the fibers, their inter-connectivity, presence of defects, arrangement, incorporation of fillers, degree of crystallinity, etc. [65, 66]. The results from the tensile tests of the electrospun PVDF webs are presented in **Figure 41**. It is noticeable that the tensile strength of PVDF webs remarkably was enhanced with increased concentrations of electrospinning solutions. Compared with the electrospun PVDF membrane with 8 wt% concentration composed of only nano-sized particles, the mechanical properties of 12 wt% and 16 wt% PVDF membranes were considerably improved when the bead-on-string structure was formed such that the external load is efficiently transferred between the beads and each fiber. In case of 20 wt% PVDF membrane consisting of only nanofibers, the tensile modulus was improved but the breaking

point and elongation has been reduced significantly. When the tensile force was applied, it seems to have endured the stronger strength, but it was broken earlier. Therefore, it can be seen that the surface structures made of nanofibers and beads is more advantageous for the mechanical reinforcement.

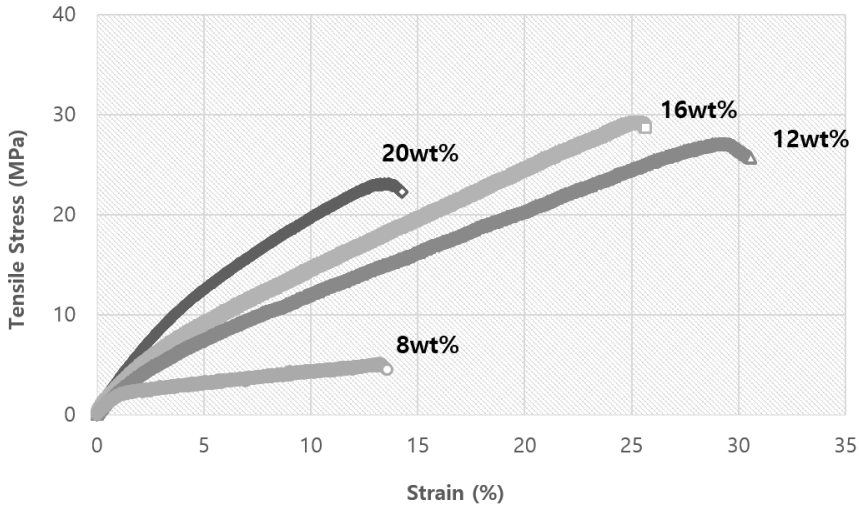

Figure 41. Stress-strain curves of the electrospun PVDF films with different concentrations.

The average tensile modulus, the ultimate tensile strength of the membranes and elongation at break are summarized in **Table 8**. The determination of the mechanical characteristics of the electrospun PVDF webs revealed that the pristine PVDF fibers had the highest values of young's modulus, tensile strength and elongation at break as well as hydrophobic property. The tensile modulus of the electrospun PVDF membranes of 12, 16, and 20 wt% concentrations were increased by 28%, 34%, and 52% respectively, compared with the 8 wt%. The tensile strength of the PVDF webs with 12 wt% and 16 wt% concentrations were 5.24 and 5.66 times greater than membrane of 8 wt%. The fiber acts as stress concentration centers where cracks initiates, and the applied tension propagates and any structure does not hinder the transfer of tension. However, in beaded fiber structures, the beads act as filler which deliver the tensile stress, then the elongation had been considerably increased. In conclusions, the bead-on-string structures composed of nanofibers and microbeads, significantly improves the mechanical properties of the electrospun PVDF membranes.

Table 8. Mechanical properties of (E_t – Young's modulus; δ– elongation at break; σ_B – tensile strength) of the electropsun PVDF webs with different concentrations.

Sample	Tensile strength σ_B (MPa)	Elongation at break δ (%)	Modulus E_t (MPa)
8 wt%	5.18 ± 0.08	13.23 ± 0.89	4.19 ± 0.09
12 wt%	27.146 ± 1.017	29.39 ± 1.32	5.35 ± 0.29
16 wt%	29.336 ± 1.024	25.31 ± 1.95	5.63 ± 0.32
20 wt%	23.145 ± 1.013	13.63 ± 0.83	6.35 ± 0.25

To test the separation capability of the electrospun PVDF membrane, a surfactant-free oil (benzene)-in-water (dyed with methyl blue for easy observation) emulsion was prepared and poured onto the web. The optical image of separation process gives a direct demonstration of the superhydrophobic property of the electrospun PVDF membranes, as shown in **Figure 42**. When a mixture of benzene and water was poured onto the superhydrophobic PVDF membrane, only the oil could pass through the web and the remained water were held on the upper surface. Without any external driving force, the oil was able to quickly permeate through the fibrous PVDF membrane. In the meantime, the water droplets were demulsified once touching the fibrous membrane and the residual water was finally retained at the above.

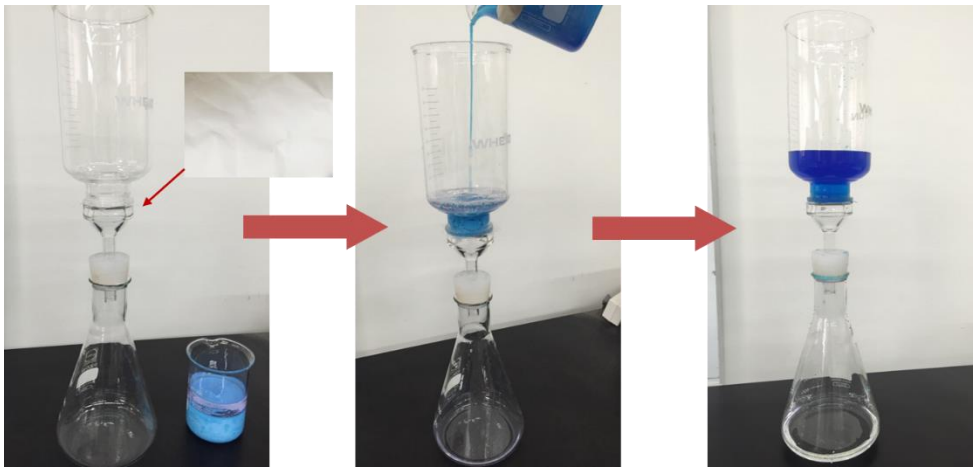

Figure 42. Separation apparatus and process of the oil-water (water dyed with methyl blue) emulsions for the electrospun PVDF membrane.

As shown in **Figure 43**, before and after filtration, the color change of the emulsion is clearly visible. Also, in microscopic images, the big oil droplets can be seen in the mixed emulsion. However, no visible water droplets could be detected in the

permeated water, indicating a high water–oil separation efficiency of the fibrous PVDF membranes for oil-in-water emulsions. The particle size distribution analysis demonstrates this results, showing the average particle size of the emulsion before the separation is about 208 µm and that of the permeated emulsion is about 0.01 µm. Therefore, it can be concluded that the murky emulsion was separated into very clean water.

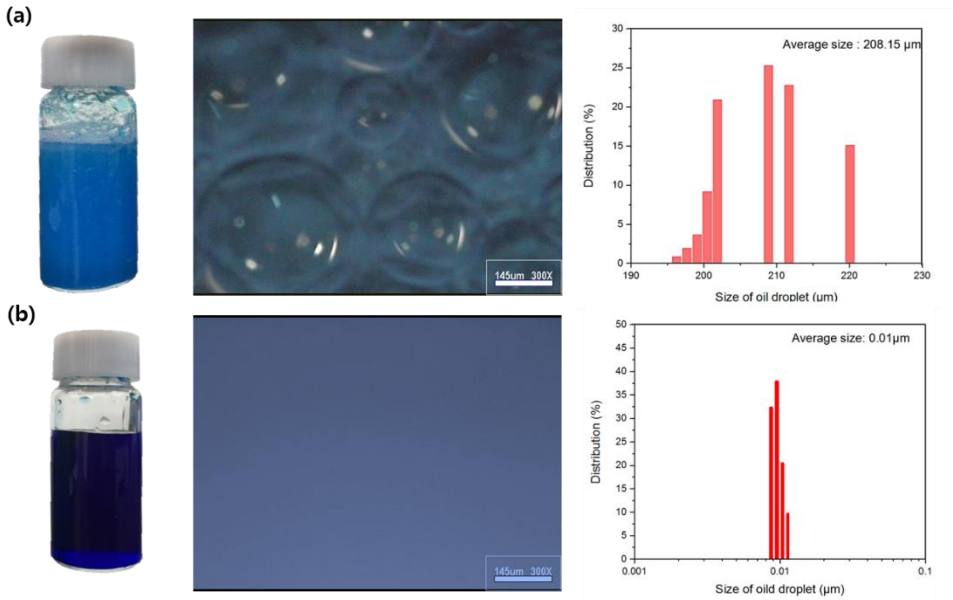

Figure 43. Optical and microscopic images of oil-in-water emulsion before (a) and after (b) filtration and their particle size distribution.

A series of experiments were carried out to investigate the oil absorption capability of the superhydrophobic PVDF membrane fabricated by electrospinning (**Figure 44**). The electrospun PVDF membrane showed excellent selective absorption for the removal of oil from water. When a piece of the electrospun membrane touched the oil layer (dyed with Oil Red) on the water surface, it only absorbed oil in emulsion within several seconds, resulting in a clean water region without any oil

layer (**Figure 44 (e)**). The excellent oil absorption capability of the electrospun membrane is mainly due to its superhydrophobicity, which were obtained by electrospinning process. The absorbed oil dissolved in ethanol solvent can be collected just by a simple evaporation process and the recycled membrane can be reused after drying.

The oil absorption capacity of the superhydrophobic PVDF membrane for benzene, silicone oil, hexadecane, and dichloromethane were 91.5, 93.7, 89.8, and 95.1%, respectively (**see Figure 45 (a)**). The variation in absorption predominantly depends on the density of oil solvents, and increasing solvent density results in higher absorption capacity. Moreover, as shown in **Figure 45 (b)**, the oil absorption capacity of the superhydrophobic PVDF membranes decreased slightly after each cycles of oil absorption cycles, demonstrating the stability of this oil sorbent material. Thus, the superhydrophobic PVDF membrane is applicable for the industrial oil-polluted water treatment as well as oil spill cleanup.

Laminating process is the well-known textile finishing technique designed to add or improve the specific function. In lamination procedure, a pre-made or extruded film is bonded onto the substrate, generally with thermal treatment or adhesive bonding. However, if a nanofiber web is spun by electrospinning over a textile fabric such as nylon or polyester, a fashion textile that exhibits various functions without being subjected to a lamination process can be produced. That is, if the nanofibrous PVDF web of thickness less than 100μm is electrospun onto a conventional textile fabric, the fashion textiles with hydrophobicity and improved mechanical or functional properties could be produced in mass production using effective electrospinning process.

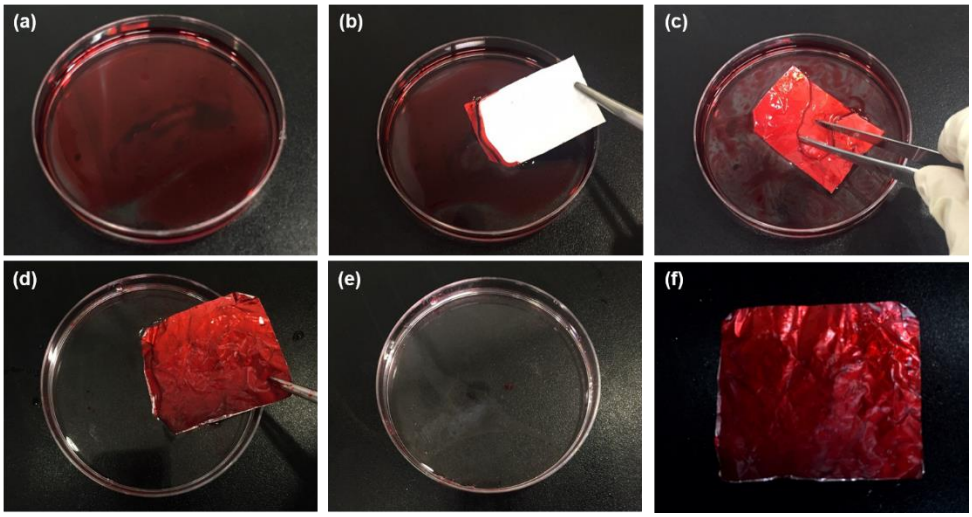

Figure 44. A series of photographs for the oil (dyed with Oil Red) absorption from the water (a-f) by the electrospun superhydrophobic PVDF membrane.

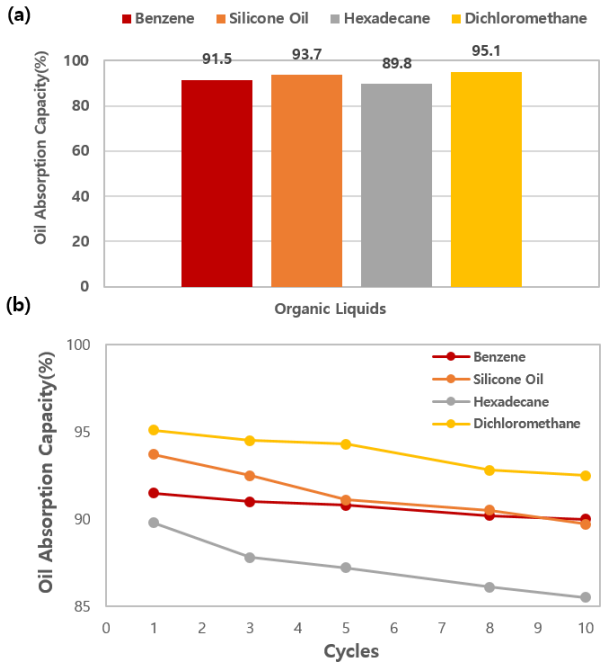

Figure 45. (a) Oil-absorption capacities of the electrospun PVDF membrane for the different oil type; (b) Oil-absorption capability changes ranging from 1 to 10 cycles.

Figure 46 shows the photographs of water droplets with the three different volumes, 3, 5, 10 µl on an electrospun PVDF films with 16wt% concentrations. For the better visualization, the water was colored with a Methylene Blue solution. As seen, the droplets preserved their spherical shape and were not absorbed after their contact with the hydrophobic film. Also, with increasing volume of the water droplets, the electrospun PVDF films did not get wet at all and retained a spherical shape.

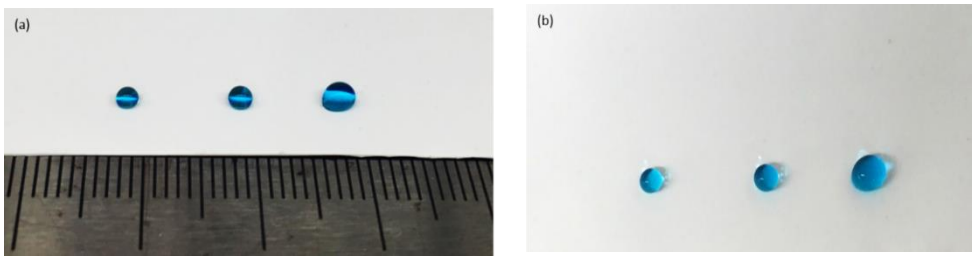

Figure 46. Photographs of water droplets with the three different volumes, 3, 5, 10 µl from the left to the right on an electrospun PVDF films with 16wt% concentrations. (a) side view; (b) top-down view.

3.4 Summary

We have successfully obtained the superhydrophobic webs from the electrospinning process of the poly(vinylidene fluoride) (PVDF) solutions by controlling the surface roughness affected by the viscosity of the electrospinning solutions. The electrospun PVDF web with the hierarchical morphology of both nanometer- and micrometer-sized structures was well fabricated using simple electrospinning system and the exhibited superhydrophobic properties with the high contact angles over 150°, the tilting angle as 10°, and the hysteresis about 11°, and good water repellency. The highly water-repellent pure PVDF membranes can be fabricated by the electrospinning without any surface modification treatment and the surface morphology and diameter of the fibers and beads of the electrospun PVDF films were significantly affected by the concentrations i.e., the viscosity of the PVDF solutions. The bead-on-string structures are more effective to be hydrophobic than the only nanofiber structures. Furthermore, bead and fiber network structure significantly improves the mechanical properties of the electrospun PVDF membranes. This electrospun PVDF membranes also have the excellent oil-water separation ability and oil absorption capability, demonstrating the stability of this oil sorbent material. Thus, our electrospun superhydrophobic PVDF membrane is a good candidate in industrial oil-polluted water treatment and oil spill cleanup.

Ⅳ. Concluding Remarks

We have successfully obtained the extremely water-repellent surfaces on cotton fabrics by introducing the hierarchical morphology of both nanometer- and micrometer-sized roughness formed from hydrophobized silica nanoparticles. The coated cotton textiles in methanol exhibited the high contact angles, the low hysteresis, and good water repellency. The factors which determines the hydrophobicity of the coatings in the different alcohol solvent are the differences in surface roughness as well as surface energy of the fabric. To achieve superhydrophobicity, the presence of hierarchical surface topology has proven to be effective. The superhydrophobic and transparent coatings can be fabricated by the spray-coating method. This approach is applicable to a variety of surfaces including textile fabrics, paper, wood, etc. but needs to be overcome the durability issues.

We have successfully obtained the superhydrophobic webs from the electrospinning process of the poly(vinylidene fluoride) (PVDF) solutions by controlling the surface roughness affected by the viscosity of the electrospinning solutions. The electrospun PVDF web with the hierarchical morphology of both nanometer- and micrometer-sized structures was well fabricated and exhibited superhydrophobic properties and good water repellency. The highly water-repellent pure PVDF membranes can be fabricated by the electrospinning without any surface modification treatment. The bead-on-string structures are more effective to be hydrophobic than the only nanofiber structures and significantly improve the mechanical properties of the electrospun PVDF membranes. This electrospun PVDF membranes also have the excellent oil-water separation ability and oil absorption capability, demonstrating the stability of this oil sorbent material. Thus, our electrospun superhydrophobic PVDF membrane is a good candidate in industrial oil-polluted water treatment and oil spill cleanup.

References

1. Nuraje, N., Khan, W. S., Lei, Y., Ceylan, M., & Asmatulu, R. (2013). Superhydrophobic electrospun nanofibers. *Journal of Materials Chemistry A*, *1*(6), 1929-1946.

2. Ji, J., Fu, J., & Shen, J. (2006). Fabrication of a superhydrophobic surface from the amplified exponential growth of a multilayer. *Advanced Materials*, *18*(11), 1441-1444.

3. Neinhuis, C., & Barthlott, W. (1997). Characterization and distribution of water-repellent, self-cleaning plant surfaces. *Annals of botany*, *79*(6), 667-677.

4. Koch, K., Bhushan, B., Jung, Y. C., & Barthlott, W. (2009). Fabrication of artificial Lotus leaves and significance of hierarchical structure for superhydrophobicity and low adhesion. *Soft Matter*, *5*(7), 1386-1393.

5. Onda, T., Shibuichi, S., Satoh, N., & Tsujii, K. (1996). Super-water-repellent fractal surfaces. *Langmuir*, *12*(9), 2125-2127.

6. Chen, W., Fadeev, A. Y., Hsieh, M. C., Öner, D., Youngblood, J., & McCarthy, T. J. (1999). Ultrahydrophobic and ultralyophobic surfaces: some comments and examples. *Langmuir*, *15*(10), 3395-3399.

7. Wu, Y. U. N. Y. I. N. G., Sugimura, H., Inoue, Y., & Takai, O. (2002). Thin Films with Nanotextures for Transparent and Ultra Water-Repellent Coatings Produced from Trimethylmethoxysilane by Microwave Plasma CVD. *Chemical Vapor Deposition*, *8*(2), 47-50.

8. Tsujii, K., Yamamoto, T., Onda, T., & Shibuichi, S. (1997). Superölabstoßende Oberflächen. *Angewandte Chemie*, *109*(9), 1042-1044.

9. Tadanaga, K., Katata, N., & Minami, T. (1997). Formation Process of Super-Water-Repellent Al2O3 Coating Films with High Transparency by the Sol–Gel Method. *Journal of the American Ceramic Society*, *80*(12), 3213-3216.

10. Tadanaga, K., Katata, N., & Minami, T. (1997). Formation Process of Super-Water-Repellent Al_2O_3 Coating Films with High Transparency by the Sol–Gel Method. *Journal of the American Ceramic Society*, *80*(12), 3213-3216.

11. Nakajima, A., Abe, K., Hashimoto, K., & Watanabe, T. (2000). Preparation of hard super-hydrophobic films with visible light transmission. *Thin Solid Films*, *376*(1), 140-143.

12. Bico, J., Marzolin, C., & Quéré, D. (1999). Pearl drops. *EPL (Europhysics Letters)*,

47(2), 220.

13. Li, Y., Liu, F., & Sun, J. (2009). A facile layer-by-layer deposition process for the fabrication of highly transparent superhydrophobic coatings. *Chemical communications*, (19), 2730-2732.

14. Tadanaga, K., Morinaga, J., Matsuda, A., & Minami, T. (2000). Superhydrophobic-superhydrophilic micropatterning on flowerlike alumina coating film by the sol-gel method. *Chemistry of materials*, *12*(3), 590-592.

15. Doshi, J., & Reneker, D. H. (1993, October). Electrospinning process and applications of electrospun fibers. In *Industry Applications Society Annual Meeting, 1993., Conference Record of the 1993 IEEE* (pp. 1698-1703). IEEE.

16. Quéré, D., Lafuma, A., & Bico, J. (2003). Slippy and sticky microtextured solids. *Nanotechnology*, *14*(10), 1109.

17. Gowri, S., Almeida, L., Amorim, T., Carneiro, N., Souto, A. P., & Esteves, M. F. (2010). Polymer nanocomposites for multifunctional finishing of textiles-a review. *Textile Research Journal*, *80*(13), 1290-1306.

18. Nakajima, A., Hashimoto, K., & Watanabe, T. (2001). Recent studies on super-hydrophobic films. *Monatshefte für Chemie/Chemical Monthly*, *132*(1), 31-41.

19. Ma, M., Hill, R. M., & Rutledge, G. C. (2008). A review of recent results on superhydrophobic materials based on micro-and nanofibers. *Journal of Adhesion Science and Technology*, *22*(15), 1799-1817.

20. Wenzel, R. N. (1936). Resistance of solid surfaces to wetting by water. *Industrial & Engineering Chemistry*, *28*(8), 988-994.

21. Quéré, D. (2008). Wetting and roughness. *Annu. Rev. Mater. Res.*, *38*, 71-99.

22. Bahners, T., Textor, T., Opwis, K., & Schollmeyer, E. (2008). Recent approaches to highly hydrophobic textile surfaces. *Journal of Adhesion Science and Technology*, *22*(3-4), 285-309.

23. Cassie, A. B. D., & Baxter, S. (1944). Wettability of porous surfaces. *Transactions of the Faraday Society*, *40*, 546-551.

24. Shirtcliffe, N. J., McHale, G., Atherton, S., & Newton, M. I. (2010). An introduction to superhydrophobicity. *Advances in colloid and interface science*, *161*(1), 124-138.

25. Xu, X., & Wang, X. (2013). The modified Cassie's equation and contact angle hysteresis. Colloid and Polymer Science, 291(2), 299-306.

26. Liu, H., Gao, S. W., Cai, J. S., He, C. L., Mao, J. J., Zhu, T. X., ... & Al-Deyab, S. S. (2016). Recent Progress in Fabrication and Applications of Superhydrophobic

Coating on Cellulose-Based Substrates. Materials, 9(3), 124.

27. Zhang, X., Shi, F., Niu, J., Jiang, Y., & Wang, Z. (2008). Superhydrophobic surfaces: from structural control to functional application. *Journal of Materials Chemistry*, *18*(6), 621-633.

28. Pan, S., Kota, A. K., Mabry, J. M., & Tuteja, A. (2012). Superomniphobic surfaces for effective chemical shielding. *Journal of the American Chemical Society*, *135*(2), 578-581.

29. Wang, Y., Xue, J., Wang, Q., Chen, Q., & Ding, J. (2013). Verification of icephobic/anti-icing properties of a superhydrophobic surface. *ACS applied materials & interfaces*, *5*(8), 3370-3381.

30. Shirtcliffe, N. J., McHale, G., Newton, M. I., & Zhang, Y. (2009). Superhydrophobic copper tubes with possible flow enhancement and drag reduction. *ACS applied materials & interfaces*, *1*(6), 1316-1323.

31. Ju, J., Xiao, K., Yao, X., Bai, H., & Jiang, L. (2013). Bioinspired conical copper wire with gradient wettability for continuous and efficient fog collection. *Advanced Materials*, *25*(41), 5937-5942.

32. Li, J., Jing, Z., Zha, F., Yang, Y., Wang, Q., & Lei, Z. (2014). Facile spray-coating process for the fabrication of tunable adhesive superhydrophobic surfaces with heterogeneous chemical compositions used for selective transportation of microdroplets with different volumes. *ACS applied materials & interfaces*, *6*(11), 8868-8877.

33. Wang, T., Hu, X., & Dong, S. (2007). A general route to transform normal hydrophilic cloths into superhydrophobic surfaces. *Chemical Communications*, (18), 1849-1851.

34. Zhou, X., Zhang, Z., Xu, X., Guo, F., Zhu, X., Men, X., & Ge, B. (2013). Robust and durable superhydrophobic cotton fabrics for oil/water separation. ACS applied materials & interfaces, 5(15), 7208-7214.

35. Li, S., & Jinjin, D. (2007). Improvement of hydrophobic properties of silk and cotton by hexafluoropropene plasma treatment. Applied Surface Science, 253(11), 5051-5055.

36. Zhao, Y., Tang, Y., Wang, X., & Lin, T. (2010). Superhydrophobic cotton fabric fabricated by electrostatic assembly of silica nanoparticles and its remarkable buoyancy. Applied Surface Science, 256(22), 6736-6742.

37. Xue, C. H., Jia, S. T., Zhang, J., & Tian, L. Q. (2009). Superhydrophobic surfaces on cotton textiles by complex coating of silica nanoparticles and hydrophobization.

Thin Solid Films, 517(16), 4593-4598.

38. Yang, J., Tang, Y., Xu, J., Chen, B., Tang, H., & Li, C. (2015). Durable superhydrophobic/superoleophilic epoxy/attapulgite nanocomposite coatings for oil/water separation. Surface and Coatings Technology, 272, 285-290.

39. Sas, I., Gorga, R. E., Joines, J. A., & Thoney, K. A. (2012). Literature review on superhydrophobic self-cleaning surfaces produced by electrospinning. Journal of Polymer Science Part B: Polymer Physics, 50(12), 824-845.

40. Ke, P., Jiao, X. N., Ge, X. H., Xiao, W. M., & Yu, B. (2014). From macro to micro: structural biomimetic materials by electrospinning. RSC Advances, 4(75), 39704-39724.

41. Li, H., Xu, Y., Xu, H., & Chang, J. (2014). Electrospun membranes: control of the structure and structure related applications in tissue regeneration and drug delivery. Journal of Materials Chemistry B, 2(34), 5492-5510.

42. Singh, A., Steely, L., & Allcock, H. R. (2005). Poly [bis (2, 2, 2-trifluoroethoxy) phosphazene] superhydrophobic nanofibers. *Langmuir*, *21*(25), 11604-11607.

43. Ma, M., Mao, Y., Gupta, M., Gleason, K. K., & Rutledge, G. C. (2005). Superhydrophobic fabrics produced by electrospinning and chemical vapor deposition. Macromolecules, 38(23), 9742-9748.Lin, J., Cai, Y., Wang, X., Ding, B., Yu, J., & Wang, M. (2011). Fabrication of biomimetic superhydrophobic surfaces inspired by lotus leaf and silver ragwort leaf. *Nanoscale*, *3*(3), 1258-1262.

44. Jiang, L., Zhao, Y., & Zhai, J. (2004). A lotus-leaf-like superhydrophobic surface: a porous microsphere/nanofiber composite film prepared by electrohydrodynamics. Angewandte Chemie, 116(33), 4438-4441.

45. Liu, F., Hashim, N. A., Liu, Y., Abed, M. M., & Li, K. (2011). Progress in the production and modification of PVDF membranes. Journal of Membrane Science, 375(1), 1-27.

46. Doyle, J. J., Choudhari, S., Ramakrishna, S., & Babu, R. P. (2013, December). Electrospun Nanomaterials: Biotechnology, Food, Water, Environment, and Energy. In Conference Papers in Science (Vol. 2013). Hindawi Publishing Corporation.

47. Choi, Y. S., Kang, H., Kim, D. G., Cha, S. H., & Lee, J. C. (2014). Mussel-inspired dopamine-and plant-based cardanol-containing polymer coatings for multifunctional filtration membranes. ACS applied materials & interfaces, 6(23), 21297-21307.

48. Correia, D. M., Ribeiro, C., Sencadas, V., Botelho, G., Carabineiro, S. A. C., Ribelles, J. G., & Lanceros-Méndez, S. (2015). Influence of oxygen plasma treatment

parameters on poly (vinylidene fluoride) electrospun fiber mats wettability. *Progress in Organic Coatings*, *85*, 151-158.

49. Chen, Y., & Kim, H. (2009). Preparation of superhydrophobic membranes by electrospinning of fluorinated silane functionalized poly (vinylidene fluoride). *Applied surface science*, *255*(15), 7073-7077.

50. Wang, S., Li, Y., Fei, X., Sun, M., Zhang, C., Li, Y., & Hong, X. (2011). Preparation of a durable superhydrophobic membrane by electrospinning poly (vinylidene fluoride)(PVDF) mixed with epoxy–siloxane modified SiO_2 nanoparticles: a possible route to superhydrophobic surfaces with low water sliding angle and high water contact angle. *Journal of colloid and interface science*, *359*(2), 380-388.

51. Ganesh, V. A., Nair, A. S., Raut, H. K., Tan, T. T. Y., He, C., Ramakrishna, S., & Xu, J. (2012). Superhydrophobic fluorinated POSS–PVDF-HFP nanocomposite coating on glass by electrospinning. *Journal of Materials Chemistry*, *22*(35), 18479-18485.

52. Zhang, J., Song, Z., Li, B., Wang, Q., & Wang, S. (2013). Fabrication and characterization of superhydrophobic poly (vinylidene fluoride) membrane for direct contact membrane distillation. *Desalination*, *324*, 1-9.

53. Tao, M., Liu, F., & Xue, L. (2012). Hydrophilic poly (vinylidene fluoride)(PVDF) membrane by in situ polymerisation of 2-hydroxyethyl methacrylate (HEMA) and micro-phase separation. *Journal of Materials Chemistry*, *22*(18), 9131-9137.

54. Hu, M. X., Li, J. N., Zhang, S. L., Li, L., & Xu, Z. K. (2014). Hydrophilic modification of PVDF microfiltration membranes by adsorption of facial amphiphile cholic acid. *Colloids and Surfaces B: Biointerfaces*, *123*, 809-813.

55. Zheng, Z., Gu, Z., Huo, R., & Ye, Y. (2009). Superhydrophobicity of polyvinylidene fluoride membrane fabricated by chemical vapor deposition from solution. *Applied Surface Science*, *255*(16), 7263-7267.

56. Deitzel, J. M., Kleinmeyer, J., Harris, D. E. A., & Tan, N. B. (2001). The effect of processing variables on the morphology of electrospun nanofibers and textiles. *Polymer*, *42*(1), 261-272.

57. Torres-Giner, S., Ocio, M. J., & Lagaron, J. M. (2008). Development of Active Antimicrobial Fiber-Based Chitosan Polysaccharide Nanostructures using Electrospinning. *Engineering in Life Sciences*, *8*(3), 303-314.

58. Extrand, C. W. (2003). Contact angles and hysteresis on surfaces with chemically heterogeneous islands. *Langmuir*, *19*(9), 3793-3796.

59. Liao, Y., Wang, R., & Fane, A. G. (2013). Engineering superhydrophobic surface on poly (vinylidene fluoride) nanofiber membranes for direct contact membrane

distillation. *Journal of membrane science*, *440*, 77-87.

60. Wang, M., Fang, D., Wang, N., Jiang, S., Nie, J., Yu, Q., & Ma, G. (2014). Preparation of PVDF/PVP core–shell nanofibers mats via homogeneous electrospinning. Polymer, 55(9), 2188-2196.

61. Nasir, M., Matsumoto, H., Danno, T., Minagawa, M., Irisawa, T., Shioya, M., & Tanioka, A. (2006). Control of diameter, morphology, and structure of PVDF nanofiber fabricated by electrospray deposition. Journal of Polymer Science Part B: Polymer Physics, 44(5), 779-786.

62. Gonçalves, R., Martins, P. M., Caparrós, C., Martins, P., Benelmekki, M., Botelho, G., & Barandiarán, J. M. (2013). Nucleation of the electroactive β-phase, dielectric and magnetic response of poly (vinylidene fluoride) composites with Fe_2O_3 nanoparticles. Journal of Non-Crystalline Solids, 361, 93-99.

63. Na, H., Chen, P., Wong, S. C., Hague, S., & Li, Q. (2012). Fabrication of PVDF/PVA microtubules by coaxial electrospinning. Polymer, 53(13), 2736-2743.

64. Gomes, J., Nunes, J. S., Sencadas, V., & Lanceros-Méndez, S. (2010). Influence of the β-phase content and degree of crystallinity on the piezo-and ferroelectric properties of poly (vinylidene fluoride). Smart Materials and Structures, 19(6), 065010.

65. Wong, S. C., Baji, A., & Leng, S. (2008). Effect of fiber diameter on tensile properties of electrospun poly (ε-caprolactone). Polymer, 49(21), 4713-4722.

66. Chen, F., Su, Y., Mo, X., He, C., Wang, H., & Ikada, Y. (2009). Biocompatibility, alignment degree and mechanical properties of an electrospun chitosan–P (LLA-CL) fibrous scaffold. Journal of Biomaterials Science, Polymer Edition, 20(14), 2117-2128.

초 록

마이크로 및 나노크기의 계층적 구조를 가진 표면의 발수 특성 및 초소수성 구현

서울대학교 대학원

공과대학 재료공학부

정선아

초소수성(Superhydrophobicity)은 물 접촉각이 150도 이상으로 물에 젖지 않는 특성으로 대표적인 예로 연잎(Lotus Leaf)을 들 수 있다. 마이크로 돌기 위에 왁스성분의 나노 돌기를 가지고 있는 연잎 위로 물방울이 젖지 않고 구르면서 표면에 이물질을 제거하는 자가세정(self-cleaning)작용을 일으키고, 이 연잎 효과는 기초연구로써의 가치뿐만 아니라, 각종 산업계에서 큰 활용가치를 가지므로 이를 모방하는 나노생체모사(nano-biomimetics)기술이 큰 각광을 받고 있다.

그동안 발표된 여러 연구에서 사용된 고가의 장비나 특수 물질의 사용 없이 짧은 시간에 간단한 제조 공정으로 계층 구조를 갖는 초소수성 표면을 제조하기 위한 목적으로 본 연구에서는 소수성 물질을 처리한 실리카 나노파티클을 면직물에 스프레이 코팅하여 초소수성 표면을 제조하였고 전기방사를 통해 초소수성의 폴리불화비닐리덴(Polyvinylidene) 웹을 제조하였다. 이들의 마이크로 나노사이즈의 이중 계층 구조를 조절하여 그에 따른 초소수성과 발수성을 비교 분석하였다.

우선, trichlorododecylsilane을 실리카 나노 입자에 처리하여 직물의 표면 에너지를 낮추었고 소수성 실리카 나노 입자를 함유한 알콜 현탁액을 면직물에 스프레이 분무함으로써 소수성의 코팅층이 섬유 직물 상에 형성되었다. 이 때, 3가지 유형의 알코올 용매를 사용하였는데 메탄올에서 처리된 면 직물에서만 마이크로 및 나노 사이즈의 이중 계층 구조가 형성되었고 170° 이상의 물 접촉각 및 10° 미만의 접촉각 히스테리시스를 보이며 극도의 발

수성을 나타냈다. 즉, 초소수성을 발현하기 위해서 낮은 표면 에너지의 이중 계층 구조를 설계하는 것이 필수적인 것임이 판명되었다. 간단한 스프레이 코팅 방식으로 초발수송의 면직물을 제조하였지만, 실리카 파티클과 면 사이에는 화학적 결합이 아니라 물리적 결합으로 붙어있어 내구성에는 문제가 있었다.

이어서, 내구력이 우수한 초소수성의 표면을 제작하기 위해 전기방사(Electrospinning) 기술을 이용하였다. 전기방사법은 정전기력에 의해 낮은 점도 상태의 고분자 용액을 순간적으로 나노사이즈의 섬유형태로 방사하여 초소수성의 표면과 비슷한 표면을 쉽게 제조할 수 있는 장점이 있어 각광받고 있다. 표면 에너지가 낮은 폴리머 중이 가장 낮다고 알려진 플루오린 화 폴리머 중에서 내구성과 기계적 특성이 우수하다고 알려진 poly(vinylidene fluoride)(PVDF)를 방사하여 초소수성 웹을 제조하고자 하였다. PVDF의 농도를 DMF 용매에 8, 12, 16, 20wt%로 용해시키고, 그에 따른 소수성과 기계적 특성을 비교 분석 하였다. 낮은 농도에서는 나노파티클로 이루어진 구조, 증가된 농도에서는 나노 섬유와 비드가 연결된 bead-on-fiber 구조가 형성되었고 높은 농도에서는 두꺼운 섬유만 이루어진 구조가 형성되었다. Bead-on-fiber 구조에서 나노사이즈의 섬유와 마이크로 크기의 비드로 형성된 이중 계층적 구조가 잘 형성되었고, 이 웹은 약 150° 의 접촉각, 접촉각 이력은 11° 로 우수한 발수성을 나타냈다. 농도 즉, 점도를 조절하면서 표면 구조를 제어하였고 이중 계층 구조를 구현하면서 전기방사 공정만으로 초소수성을 갖는 표면을 제조하였다. 또한 훌륭한 유수 분리 성능 및 흡유 능력을 나타내어 오일 흡착 재료로서의 안정성도 입증하였다. 우수한 기계적 및 내구력을 지닌 초소수성 PVDF 멤브레인은 산업용 오일 오염 처리 및 오일 유출 정화에 적용될 것으로 기대된다.

주요어: 초소수성, 나노파티클, 스프레이코팅, 전기방사

학 번: 2012-24166